Spectrochimica Acta Part A: Molecular and Biomolecular Spectroscopy 312 (2024) 124011

Contents lists available at ScienceDirect

Spectrochimica Acta Part A: Molecular and Biomolecular Spectroscopy

journal homepage: www.journals.elsevier.com/spectrochimica-acta-part-a-molecular-and-biomolecular-spectroscopy

FT-spectroscopy of the $^{12}C^{18}O$ rare isotopologue and deperturbation analysis of the $A^1\Pi(v = 3)$ level

M.I. Malicka [a,*], R.W. Field [b], S. Ryzner [c,d], A. Stasik [c], W. Ubachs [e], A.N. Heays [f], N. de Oliveira [g], W. Szajna [c], R. Hakalla [c]

[a] The Faculty of Mathematics and Applied Physics, Rzeszów University of Technology, Powstańców Warszawy 8 Street, 35-959, Rzeszów, Poland
[b] Department of Chemistry, Massachusetts Institute of Technology, Cambridge MA02139, USA
[c] Materials Spectroscopy Laboratory, Institute of Physics, University of Rzeszów, Pigonia 1 Street, 35-310 Rzeszów, Poland
[d] Doctoral School of the University of Rzeszów, University of Rzeszów, Rejtana 16C Street, 35-959 Rzeszów, Poland
[e] Department of Physics and Astronomy, and LaserLaB, Vrije Universiteit, De Boelelaan 1081, 1081 HV Amsterdam, the Netherlands
[f] J. Heyrovský Institute of Physical Chemistry, Dolejškova 2155/3, 182 23 Prague 8, Czech Republic
[g] Synchrotron SOLEIL, Orme de Merisiers, St. Aubin, BP 48, F-91192 Gif sur Yvette Cedex, France

HIGHLIGHTS

- VUV-FT and VIS-FT complementary, high-resolution techniques were used for registration of 5 ro-vibronic bands in $^{12}C^{18}O$.
- The deperturbation analysis of the $A^1\Pi(v = 3)$ level in $^{12}C^{18}O$ based on 571 line frequencies was performed.
- A significant, indirect $a^3\Pi(v = 14) \sim e^3\Sigma^-(v = 6) \sim A^1\Pi(v = 3)$ and $a'^3\Sigma^+(v = 14) \sim A^1\Pi(v = 3) \sim e^3\Sigma^-(v = 6)$ influences were detected.
- Within the $^{12}C^{18}O$ $A^1\Pi(v = 3)$ level, 5 newly observed spin–orbit and rotation-electronic interactions were analysed.
- 112 ro-vibronic term values of the $A^1\Pi(v = 3, J_{max} = 55)$, $a'^3\Sigma^+(v = 13)$, $D^1\Delta(v = 4)$ and $I^1\Sigma^-(v = 5)$ levels were determined..

GRAPHICAL ABSTRACT

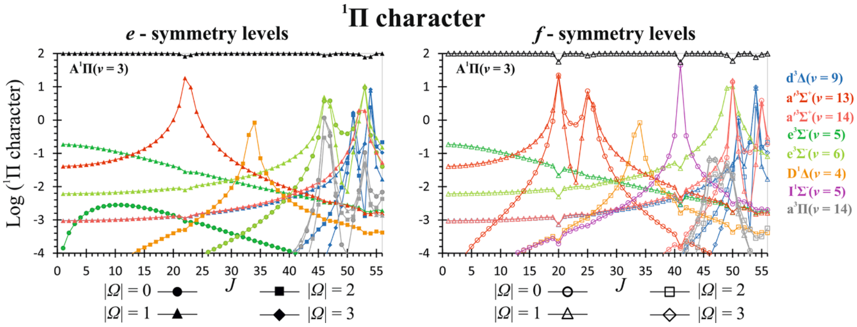

ARTICLE INFO

Keywords:
High-resolution VUV-FT synchrotron spectroscopy
High-resolution Vis-FT emission spectroscopy
Carbon monoxide
$^{12}C^{18}O$ isotopologue
Deperturbation analysis

ABSTRACT

Research on $^{12}C^{18}O$ was carried out using two complementary Fourier-transform methods: *(1)* vacuum-ultraviolet absorption spectroscopy, with an accuracy ca. 0.03 cm^{-1} on the DESIRS beamline (SOLEIL synchrotron) and *(2)* visible emission spectroscopy with an accuracy of about 0.005–0.007 cm^{-1} by means of the Bruker IFS 125HR spectrometer (University of Rzeszów). The maximum rotational quantum number of the energy levels involved in the observed spectral lines was $J_{max} = 54$. An effective Hamiltonian and the term-value fitting approach were implemented for the precise analysis of the $A^1\Pi(v = 3)$ level in $^{12}C^{18}O$. It was performed by means of the PGOPHER code. The data set consisted of 571 spectral lines belonging to the $A^1\Pi$ - $X^1\Sigma^+(3, 0)$, $B^1\Sigma^+$ - $A^1\Pi(0, 3)$, $C^1\Sigma^+$ - $A^1\Pi(0, 3)$ bands and several lines involving states that perturb the $A^1\Pi(v = 3)$ level as well as to the previously analysed $B^1\Sigma^+$ - $X^1\Sigma^+(0, 0)$ and $C^1\Sigma^+$ - $X^1\Sigma^+(0, 0)$ transitions. A significantly extended

---

[*] Corresponding author.
E-mail address: m.malicka@prz.edu.pl (M.I. Malicka).

https://doi.org/10.1016/j.saa.2024.124011
Received 1 December 2023; Received in revised form 1 February 2024; Accepted 5 February 2024

quantum–mechanical description of the $A^1\Pi(v = 3)$ level in $^{12}C^{18}O$ was provided. It consists of the 5 new unimolecular interactions of the spin–orbit and rotation-electronic nature, which had not been taken into account previously in the literature. The ro-vibronic term values of the $A^1\Pi(v = 3, J_{max} = 55)$, $a'^3\Sigma^+(v = 13)$, $D^1\Delta(v = 4)$ and $I^1\Sigma^-(v = 5)$ levels were determined with precision improved by a factor of 10 relative to the previously known values.

1. Introduction

The carbon monoxide (CO) molecule is the second-most abundant interstellar molecule after molecular hydrogen. However, because H_2 is difficult to observe directly, carbon monoxide is used as a tracer of it [1] and other molecular gases in molecular clouds [2], protoplanetary disks [3] and galaxies [4]. In the interstellar medium (ISM), CO is a precursor to the formation of polyatomic molecules [5], which dominate and control many chemical reactions in gas phase processes [6]. CO has been observed in the spectra of galaxies [7,8], comets [9], inter-galactic molecular clouds [10], the Sun [11], and also in the atmospheres of planets [12,13] and exoplanets [14]. CO has also been used as a probe to look for variability in fundamental constants in the early Universe [15–18], study of the physical conditions of the nebulae gases via the electronic transitions (e.g. $A^1\Pi$ - $X^1\Sigma^+$ in ρ-Ophiuchi, [19–21], as well as in creating models of aurora and airglow emission from planetary atmospheres (e.g. in the upper atmosphere of Venus [22]). Because of the demand for ultra-accurate standards for the models of the Earth's atmosphere, the abundance of the CO molecule plays an important role in modelling the processes taking place there [23–25].

Due to the occurrence of perturbations resulting from spin-orbit and ***L* -** uncoupling interactions, the effects of centrifugal distortion, as well as the mixing with highly-excited Rydberg states, carbon monoxide plays a significant role in modelling unimolecular dynamics [26–32]. The first excited singlet electronic state of CO ($A^1\Pi$) is among the most interesting due to the numerous multistate perturbations that appear within it. These perturbations are caused by the ro-vibrational levels of the $e^3\Sigma^-$, $a'^3\Sigma^+$, $d^3\Delta$ triplet states and the $I^1\Sigma^-$ and $D^1\Delta$ singlet states [33–36] as well as indirectly by the $a^3\Pi$ state [37,38].

In the rare $^{12}C^{18}O$ isotopologue, the deperturbation analyses of the $A^1\Pi$ state were performed by Haridass et al. [39], Beaty et al. [40], Trivikram et al. [41], and Malicka et al. [37,42]. Haridass et al. [39] conducted an analysis for the $A(v = 1$ and $2)$ levels based on measurements of the $A^1\Pi$ - $X^1\Sigma^+$ system with an accuracy of 0.1 cm^{-1},using a grating 10.6 m vacuum spectrograph, whereas Beaty et al. [40] carried out a deperturbation analysis for the $A(v = 0$–$9)$ levels using the supersonic jet expansion technique for determination of the $A^1\Pi$ - $X^1\Sigma^+$ bands, at an accuracy of 0.05–0.2 cm^{-1}. In these two analyses, only the strongest unimolecular interactions had been considered. We performed an extended deperturbation analysis of the $A^1\Pi$ state in $^{12}C^{18}O$ based on the $A^1\Pi$ - $X^1\Sigma^+$, $B^1\Sigma^+$ - $A^1\Pi$, $C^1\Sigma^+$ - $A^1\Pi$, $B^1\Sigma^+$ - $X^1\Sigma^+$ and $C^1\Sigma^+$ - $X^1\Sigma^+$ systems using several different combinations of modern spectroscopic techniques: two-photon Doppler-free laser methodology (LaserLab Amsterdam), vacuum ultraviolet Fourier-transform spectroscopy (VUV-FTS) based on synchrotron radiation (DESIRS beamline, SOLEIL synchrotron), and visible Fourier-transform spectroscopy (Vis-FTS) using a Bruker IFS-125HR spectrometer (Rzeszów University) with accuracy of about 0.001 cm^{-1}, 0.01 and 0.005 cm^{-1}, respectively. The new results have provided a significantly improved description of the $A^1\Pi(v = 0$ - $2)$ levels and its perturbers in $^{12}C^{18}O$ together with their complex web of unimolecular interactions [37,41,42].

The deperturbation analysis of the $A^1\Pi(v = 3)$ level in $^{12}C^{18}O$ had been carried out only by Beaty et al. [40] so far. The results reported there are limited due to the use of spectra with an accuracy of 0.05–0.2 cm^{-1} and observed rotational levels only up to $J_{max} = 22$, and included a deperturbation analysis of only four perturbation mechanisms, i.e. $A^1\Pi(v = 3) \sim [a'^3\Sigma^+(v = 13)$, $d^3\Delta(v = 8)$, $e^3\Sigma^-(v = 5)$ and $D^1\Delta(v = 4)]$, which, moreover, were represented by the non-fitted parameters. The current work focuses on the first complete, high-accuracy deperturbation analysis of the $A^1\Pi(v = 3)$ level of $^{12}C^{18}O$, based on high-resolution spectra obtained from a combination of the VUV-FTS and Vis-FTS techniques. Our goal is to provide: *(i)* a significantly extended, improved and comprehensive set of the deperturbed molecular constants; *(ii)* perturbation parameters; and *(iii)* ro-vibronic term values of $^{12}C^{18}O$ $A^1\Pi(v = 3)$; *(iv)* and a comparison to those published in Ref. [40]. This research is a part of our team project [34–38,41–44] on a current state-of-the-art treatment of perturbations that affect the $A^1\Pi$ state of all CO isotopologues.

2. Experimental procedures

2.1. VUV-FT absorption spectroscopy (SOLEIL synchrotron)

The VUV absorption spectrum has been recorded using the VUV-FTS permanent end-station on the DESIRS beamline at the synchrotron SOLEIL facility [45,46]. The instrument has been fully described

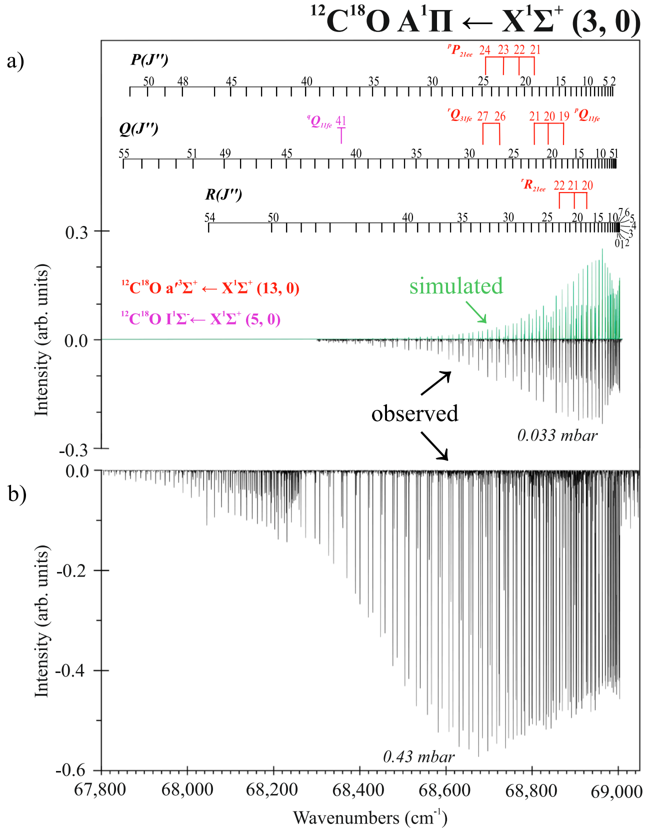

Fig. 1. Experimental spectra of the $A^1\Pi$ – $X^1\Sigma^+(3, 0)$ band with the $a'^3\Sigma^+$ - $X^1\Sigma^+(13, 0)$ and $I^1\Sigma^-$ - $X^1\Sigma^+(5, 0)$ extra-lines of $^{12}C^{18}O$ after baseline linearization and additional zero padding (lower, black traces in figure (a) and (b)). They were obtained by means of VUV-FT spectroscopy technique for two different pressures of the gas mixture. The upper, green trace presents the simulated spectrum plotted on the basis of a final deperturbation analysis using the PGOPHER software [68]. The remaining bands were considered as contaminations.

Table 1
Wavenumbers (in cm^{-1}) of the $A^1\Pi \leftarrow X^1\Sigma^+$(3, 0), VUV-FT absorption band of $^{12}C^{18}O$[a,b,c].

J"	*R*(*J*")		*Q*(*J*")		*P*(*J*")	
	σ	*u*(σ)[c]	σ	*u*(σ)[c]	σ	*u*(σ)[c]
0	68,999.17[b]	0.03				
1	69,001.33[b]	0.04	68,995.49[b]	0.03		
2	69,002.80[b]	0.04	68,994.03	0.03	68,988.16[b]	0.04
3	69,003.52[b]	0.03	68,991.81[b]	0.03	68,983.06[b]	0.06
4	69,003.50[b]	0.03	68,988.87[b]	0.03	68,977.14[b]	0.05
5	69,002.75[b]	0.03	68,985.18	0.03	68,970.59[b]	0.03
6	69,001.26[b]	0.03	68,980.77	0.03	68,963.24[b]	0.03
7	68,999.00[b]	0.03	68,975.62[b]	0.03	68,955.12[b]	0.03
8	68,996.05[b]	0.03	68,969.73[b]	0.03	68,946.32	0.03
9	68,992.33[b]	0.03	68,963.07[b]	0.03	68,936.79	0.03
10	68,987.88[b]	0.03	68,955.73[b]	0.03	68,926.51[b]	0.03
11	68,982.72[b]	0.03	68,947.63	0.03	68,915.49	0.03
12	68,976.76[b]	0.03	68,938.79	0.03	68,903.73	0.03
13	68,970.12[b]	0.03	68,929.21	0.03	68,891.24[b]	0.03
14	68,962.67[b]	0.03	68,918.88	0.03	68,878.03[b]	0.03
15	68,954.53[b]	0.03	68,907.81	0.03	68,864.01[b]	0.03
16	68,945.62	0.03	68,896.01	0.03	68,849.33[b]	0.03
17	68,935.95	0.03	68,883.44	0.03	68,833.88	0.03
18	68,925.52	0.03	68,870.08	0.03	68,817.68	0.03
19	68,914.30	0.03	68,855.82	0.03	68,800.75	0.03
20	68,902.18	0.03	68,844.16	0.03	68,783.04	0.03
21	68,888.31	0.03	68,826.51	0.03	68,764.54	0.03
22	68,878.31[b]	0.03	68,810.03	0.03	68,745.16	0.03
23	68,863.40[b]	0.03	68,792.92	0.03	68,724.02[b]	0.03
24	68,848.35	0.03	68,775.03	0.03	68,706.75	0.03
25	68,832.64	0.03	68,755.78	0.03	68,684.63	0.03
26	68,816.25	0.03	68,738.34	0.03	68,662.32	0.03
27	68,799.13	0.03	68,717.97	0.03	68,639.39	0.04
28	68,781.26	0.03	68,697.14	0.03	68,615.77	0.04
29	68,762.67	0.03	68,675.65	0.03	68,591.42	0.04
30	68,743.27[b]	0.04	68,653.41	0.04	68,566.34	0.04
31	68,723.15[b]	0.05	68,630.43	0.04	68,540.52	0.04
32	68,702.25	0.03	68,606.71	0.04	68,513.95	0.04
33	68,680.76	0.03	68,582.22	0.04	68,486.64	0.04
34	68,658.28	0.04	68,557.12	0.04	68,458.57	0.04
35	68,635.11	0.04	68,531.07	0.04	68,429.89	0.04
36	68,611.20	0.04	68,504.33	0.04	68,400.27	0.04
37	68,586.51	0.04	68,476.82	0.04	68,369.95	0.04
38	68,561.06	0.04	68,448.56	0.04	68,338.88	0.04
39	68,534.83	0.04	68,419.53	0.04	68,307.07	0.04
40	68,507.83	0.04	68,389.70	0.04	68,274.49	0.04
41	68,480.04	0.04	68,360.72	0.04	68,241.15	0.04
42	68,451.48	0.04	68,328.03	0.04	68,207.06[b]	0.04
43	68,422.09	0.04	68,295.90	0.04	68,172.18	0.04
44	68,391.80	0.04	68,263.00	0.04	68,136.54[b]	0.04
45	[d]		68,229.35[b]	0.04	68,100.09	0.04
46	68,331.04	0.04	68,194.88[b]	0.04	68,062.74[b]	0.04
47	68,297.76	0.04	68,159.59[b]	0.04	[d]	
48	68,264.26[b]	0.07	68,123.32[b]	0.06	67,987.90[b]	0.08
49	68,230.1[b]	0.2	68,085.15	0.04	67,947.6[bw]	0.4
50	–	0.07	[e]		67,907.09	0.07
51	–		68,012.86[b]	0.07	67,865.99	0.06
52	[e]		67,973.24	0.07		
53	–		67,933.1[bw]	0.5		
54	68,049.03	0.05	67,893.67	0.09		

[a] The instrumental resolution was 0.27 cm^{-1}. The absolute calibration uncertainty was 0.03 cm^{-1}. The absolute accuracy of the wavenumber measurements was estimated to be 0.03 cm^{-1}.

[b] The lines marked *b* and/or *w* are blended and/or weak (SNR < 3).

[c] One standard deviation $u(\sigma)$ represents combinations of the calibration and fitting errors of the wavenumber measurements.

[d] Unfitted because of a rapid, critical decrease of the line intensity, which is caused by the multi-state A(3) ~ e(6), a(14) ~ e(6) and a(14) ~ e(6) ~ A(3) perturbations at $J = 46$–47.

[e] Unfitted because of a decrease of the line intensity, which is caused by the multi-state A(3) ~ [e(6), a'(14)] and a'(14) ~ A(3) ~ e(6) perturbations at $J = 50$ and 52–53 for the *f*- and *e*-parity levels, respectively.

previously [37,38,41,42]. We will only present here the technical details relevant for this article. The VUV-FTS instrument allows extension of the FTS technique into the far VUV, by exploiting an all-reflective interferometer design. The instrumental resolution was set to ca. 0.27 cm^{-1} to be comparable to the Doppler width of the measured lines. A 40 cm long windowless absorption cell is heated in-vacuum by a commercial heating element (Thermocoax) [47]. Temperature regulation is based on a signal from a thermocouple connected at one end of the cell. The maximum achievable temperature is ~ 900 K [47]. The gas flow is controlled by a needle valve adjustment of the CO column density. The synchrotron beam (bandwidth $\Delta E/E = 7$ %) is reflected towards the VUV-FTS experimental branch, passes through the absorption cell before entering the spectrometer. The VUV spectra of the $^{12}C^{18}O$ $A^1\Pi$ - $X^1\Sigma^+$(3, 0) band were obtained at pressures of 0.033 and 0.43 mbar and

Table 2
Wavenumbers (in cm^{-1}) of the interaction-induced lines observed in the $A^1\Pi \leftarrow X^1\Sigma^+$ (3, 0), VUV-FT absorption band of $^{12}C^{18}O$.[a,b,c,d]

J''	$^rR_{21ee}$		$^pQ_{11fe}$		$^qQ_{11fe}$		$^rQ_{31fe}$		$^pP_{21ee}$	
	σ	$u(\sigma)$[d]	σ	$u(\sigma)$[d]	σ	$u(\sigma)$[d]	σ	$u(\sigma)$[d]	σ	$u(\sigma)$[d]
$a'^3\Sigma^+$ - $X^1\Sigma^+$ (13, 0)										
19			68,873.87	0.04						
20	68,927.65	0.04	68,838.12	0.04						
21	68,899.03	0.04	68,806.20[b]	0.04					68,806.04[b]	0.04
22	68,864.25[b]	0.04							68,770.64[b]	0.04
23									68,734.74	0.04
24									68,692.72	0.04
…										
26							68,725.20	0.04		
27							68,686.52[b]	0.06		
$I^1\Sigma^-$ - $X^1\Sigma^+$ (5, 0)										
41					68,357.40	0.04				

[a] The instrumental resolution was 0.27 cm^{-1}. The absolute calibration uncertainty was 0.03 cm^{-1}. The absolute accuracy of the wavenumber measurements was estimated to be 0.03 cm^{-1}.

[b] The lines marked *b* and/or *w* are blended and/or weak (SNR < 3).

[c] The superscripts *p*, *q*, and *r* denote change in the total angular momentum excluding spin.

[d] One standard deviation representing combinations of the calibration and fitting errors of the wavenumber measurements.

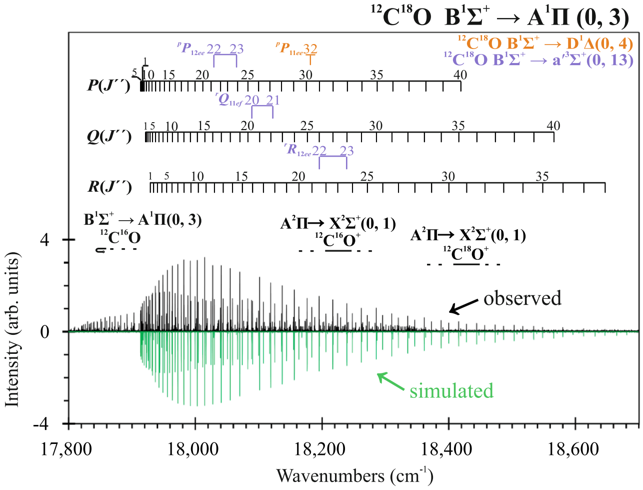

Fig. 2. Experimental spectrum of the $^{12}C^{18}O$ $B^1\Sigma^+$ - $A^1\Pi(0, 3)$ band with the $^{12}C^{18}O$ $B^1\Sigma^+$ - $D^1\Delta(0, 4)$ and $B^1\Sigma^+$ - $a'^3\Sigma^+(0, 13)$ extra-lines recorded by means of Vis-FT spectroscopy technique (upper, black trace) as well as the simulated one plotted on the basis of the final deperturbation analysis using the PGOPHER software [68] (lower, green trace).

temperature of 596 K, corresponding to measured column densities of 4 × 10^{14} and 8 × 10^{15} cm^{-2}, up to $J_{max} = 34$ and 54, respectively. The best SNR was 115:1 and 280:1 for the lower and higher pressures of the $^{12}C^{18}O$ gas. In order to analyse the spectra: *(i)* the spectra were linearised using a concave rubberband method [48]; and *(ii)* an additional zero-filling procedure with a factor of 4 was applied [49]. The spectra are presented in Fig. 1. Absolute frequency calibration was made uniformly to all measured spectra with 0.03 cm^{-1} uncertainty (1σ), as described by Malicka et al. [37,42]. The wavenumbers are collected in Table 1, and the wavenumbers of the lines involving states that perturb the $A^1\Pi(v = 3)$ level (the so-called "extra-lines") are listed in Table 2. The absolute accuracy of the wavenumber measurements was estimated to be ca. 0.03 cm^{-1}.

2.2. Vis-FT emission spectroscopy (University of Rzeszów)

The $B^1\Sigma^+$- $A^1\Pi(0, 3)$ and $C^1\Sigma^+$ - $A^1\Pi(0, 3)$ emission bands of $^{12}C^{18}O$ in the visible wavelength region, together with their extra-lines, were recorded using a 1.71-m Bruker spectrometer (IFS 125HR), located in the Materials Spectroscopy Laboratory (University of Rzeszów). The experimental setup has been described in detail elsewhere [37,41,42] and is discussed briefly here. The FT spectrometer was operated under vacuum (p < 0.01 mbar). An external source of the spectra consisted of an air-cooled, hollow-cathode (HC) lamp filled with a static $^{18}O_2$ gas at a pressure of about 3 mbar. The $^{18}O_2$ gas was provided by Sigma-Aldrich (spectral purity: 98.1 % of $^{18}O_2$ and 1.9 % of $^{16}O_2$). During the electric discharge process (780 V and 54 mA DC) [44,50,51], the O_2 molecules react with the ^{12}C atoms ejected from a drilled carbon filler placed inside the cathode, thus forming the $^{12}C^{18}O$ molecules in the plasma. In the obtained spectrum, $^{12}C^{16}O$ spectral lines appeared as well, which were treated as contaminants in the analysis process.

The $B^1\Sigma^+$ - $A^1\Pi(0, 3)$ and $C^1\Sigma^+$ - $A^1\Pi(0, 3)$ spectra of $^{12}C^{18}O$, respectively in the range of 17,900–18,700 cm^{-1} and 22,900–23,500 cm^{-1} were accumulated over 128 scans with a spectral resolution of 0.018 cm^{-1}. The spectra are presented in Figs. 2-3. The SNR was 80: 1 and 20: 1 for the $B^1\Sigma^+$ - $A^1\Pi(0, 3)$ and $C^1\Sigma^+$ - $A^1\Pi(0, 3)$ bands, respectively. The temperature of the DC-plasma was estimated to be 1100(50) K, which made it possible to observe spectral lines associated with rotational levels up to $J_{max} = 40$ for the $B^1\Sigma^+$ - $A^1\Pi(0, 3)$ band and $J_{max} = 34$ for the $C^1\Sigma^+$ - $A^1\Pi(0, 3)$ band. The spectra were calibrated with 0.004 cm^{-1} uncertainty (1σ) using the 633 nm line of an internal frequency-stabilised (±3.3•10^{-5} cm^{-1}/hour) HeNe laser. The laser line had been previously calibrated in a separate procedure using the N_2O absorption spectra of the mid infrared region (2200 cm^{-1} [52]) according to a procedure described in Ref. [53]. The absolute accuracy of the wavenumber measurements was estimated to be 0.005 cm^{-1} and 0.007 cm^{-1} for single, medium-strong lines, while for weak and/or blended lines 0.006 cm^{-1} and 0.02 cm^{-1} for the $B^1\Sigma^+$ - $A^1\Pi(0, 3)$ and $C^1\Sigma^+$ - $A^1\Pi(0, 3)$ bands, respectively. The wavenumbers of the bands are collected in Table 3 and Table 4, and the extra-lines are listed in Table 5.

3. Deperturbation analysis

3.1. Procedures

The multi-state perturbations of the CO $A^1\Pi$ state are caused directly by the ro-vibrational levels of the $e^3\Sigma^-$, $a'^3\Sigma^+$, $d^3\Delta$ triplet states and the $I^1\Sigma^-$ and $D^1\Delta$ singlet states [33–36] and indirectly by the $a^3\Pi$ state

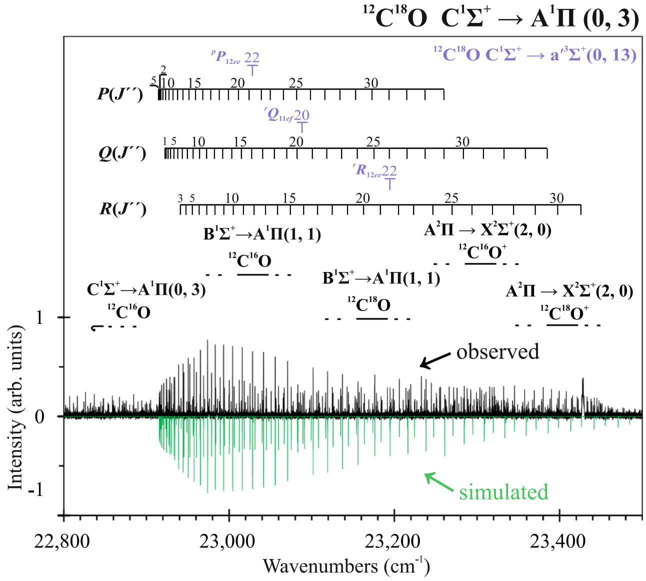

Fig. 3. Experimental spectrum of the $^{12}C^{18}O$ $C^1\Sigma^+$ - $A^1\Pi(0, 3)$ band with the $^{12}C^{18}O$ $C^1\Sigma^+$ - $a'^3\Sigma^+(0, 13)$ extra-lines recorded by Vis-FT spectroscopy technique (upper, black trace) as well as the simulated one plotted on the basis of the final deperturbation analysis using the PGOPHER software [68] (lower, green trace).

[37,38]. In order to study the $A^1\Pi(v = 3)$ level of the $^{12}C^{18}O$ isotopologue, several steps were taken. High-accuracy experimental data consisting of 389 high-resolution transitions derived from 3 bands and their extra-lines were obtained using: *(i)* VUV-FTS, $A^1\Pi$ - $X^1\Sigma^+(3, 0)$ band and *(ii)* Vis-FT spectroscopy, the $B^1\Sigma^+$ - $A^1\Pi(0, 3)$ and $C^1\Sigma^+$ - $A^1\Pi(0, 3)$ bands. Based on literature [54–66], an energy level diagram of the neighbourhood (69,000–72,500 cm^{-1}) of the $A^1\Pi(v = 3)$ level has been constructed in order to identify the levels possibly capable of perturbing this level. The diagram is presented in Fig. 4. In addition to the high-resolution lines obtained in this investigation, 182 high-accuracy transitions belonging to the $B^1\Sigma^+$ - $X^1\Sigma^+(0, 0)$ and $C^1\Sigma^+$ - $X^1\Sigma^+(0, 0)$ bands were obtained by the VUV-FTS experiment by Trivikram et al. [41] and Malicka et al. [42]. These lines were also introduced into the analysis. An experimental data set, consisting of a total of 571 high-resolution transitions, was used in the deperturbation analysis of the $A^1\Pi(v = 3)$ level in $^{12}C^{18}O$.

The deperturbation analysis was performed using an extended version of the PGOPHER program [67,68]. The $A^1\Pi(v = 3)$ level and its perturbers were represented in the model by the effective Hamiltonian, while the $B^1\Sigma^+(v = 0)$ and $C^1\Sigma^+(v = 0)$ levels were represented by their rotational term values. Details of this, the so called "term-value fitting approach", were used because of the currently unresolved issue of several very weak perturbations in the B and C Rydberg states. Description of the term value determination procedure can be found in Refs. [69–72]. The initial set of molecular constants, including the parameters of the $A^1\Pi(v = 3)$ level and its perturbers, obtained in Refs. [57,59,61,73,74], was used. The initial values of the perturbation parameters have been calculated in this work based on Refs. [34,36,57,59,73,75]. In a situation where an interaction parameter turned out to be significant for the fit, but correlated with other parameter(s) and/or statistically undetermined, its value was kept fixed. The accuracy of the fitted parameters was tested in the way described in detail in Ref. [38] (as a footnote of Table 8). During the current deperturbation analysis, 42 interactions (type of spin–orbit, spin-electronic and rotation-electronic of the $\boldsymbol{L}$-uncoupling type) were treated, 9 were included and 4 were varied. Details can be found in Table 6. The molecular constants of the $^{12}C^{18}O$ $X(v = 0)$ ground state were fixed at the values determined by Coxon and Hajigeorgiou [58]. Rotational term values of the $B^1\Sigma^+(v = 0)$ and $C^1\Sigma^+(v = 0)$ levels were fixed in the fit at the values determined by Malicka et al. [42].

The deperturbation analysis resulted in 13 independent fitted parameters: 9 deperturbed molecular constants of the $A^1\Pi(v = 3)$, $a'^3\Sigma^+(v = 13)$, $D^1\Delta(v = 4)$ and $I^1\Sigma^-(v = 5)$ levels; 2 spin–orbit interaction parameters of the $A^1\Pi(v = 3) \sim [e^3\Sigma^-(v = 6), a'^3\Sigma^+(v = 13)]$ perturbations, and 2 rotation-electronic ($\boldsymbol{L}$ - uncoupling) interaction parameters of $A^1\Pi(v = 3) \sim [I^1\Sigma^-(v = 5), D^1\Delta(v = 4)]$. The rotation-electronic interactions are described with the symbol ξ [34,35,42]. The spin–orbit and spin-electronic interaction parameters are expressed by the same symbol η, because both of them have the same Ω-dependence and it is not possible to determine them separately, thus the $\eta_{a\sim e,d,a'}$ parameter is a linear combination both of these interactions. All of the 13 fitted and 49 fixed molecular parameters, found to be meaningful in the final deperturbation fit, are listed in Table 7. During the fits, the correlations between the parameters were fully examined, based on the correlation matrix. The root-mean-square error (RMSE) of the unweighted residuals of all transitions included in the final model was 0.015 cm^{-1}. This value is within the arithmetic mean of the line position uncertainty medians in the individual bands used in the analysis (0.0043 cm^{-1} for B - A(0, 3), 0.0092 cm^{-1} for C - A(0, 3), 0.03 cm^{-1} for A - X(3, 0), 0.01 cm^{-1} for B - X(0, 0), and 0.01 cm^{-1} for C - X(0, 0)), thus the model is statistically satisfactory. Full details of the final deperturbation analysis can be found in the output (*.log) file of the PGOPHER program attached as supplementary material no. 1.

The unimolecular interactions can be also expressed by described fractional characters of the $A^1\Pi(v = 3)$, $a^3\Pi(v = 14)$, $e^3\Sigma^-(v = 6)$ and $a'^3\Sigma^+(v = 14)$ of the ro-vibrational *e*- and *f*- symmetry levels of their perturbers. The fractional characters of the analysed levels are shown in Figs. 5 and 6. The admixture of character is a percentage $C^2_{ik} \bullet 100\%$, where $C_{ik} = \langle\Phi_k|\Psi_i\rangle$ is the mixing coefficient extracted from the eigenvectors of the diagonalised energy matrix in the final fit of the deperturbation analysis.

The experiment-based, ro-vibronic term values of the $A^1\Pi(v = 3)$, $a'^3\Sigma^+(v = 13)$, $D^1\Delta(v = 4)$, and $I^1\Sigma^-(v = 5)$ levels were determined and are presented in Table 8 and 9 together with their fractional $^1\Pi$ characters. The reduced term values were calculated and highlighted in Fig. 7.

Copies of the Tables 1, 3, 4, 8 and 9 in ASCII format are included in the supplementary material no. 2.

3.2. *Indirect interactions among the $\pi^4\sigma\pi^*$ and $\pi^3\sigma^2\pi^*$ configurations of CO*

The big picture of the perturbations of the ($\pi^4\sigma\pi^*$) $A^1\Pi$ and $a^3\Pi$ states by the ($\pi^3\sigma^2\pi^*$) $a'^3\Sigma^+$, $e^3\Sigma^-$, $d^3\Delta$, $I^1\Sigma^-$, and $D^1\Delta$ states has been well known for more than 50 years [33,57,59,61,66,73–77]. All of the matrix elements between the (a and A) and the (a', e, d, I, and D) states are described by the product of a calculable vibrational integral and an electronic orbital integral [33]. Spectroscopic and molecular source technologies have improved by several orders of magnitude. Resolution, precision, and range of *J* levels have made it possible to reexamine all of the old spectra for new classes of perturbation interactions [59]. Improved sensitivity has made it possible to record spectra of all six combinations of ^{12}C, ^{13}C, ^{16}O, ^{17}O, and ^{18}O isotopes. Classes of perturbation that were too weak or poorly sampled can now be observed with redundancy and sensitivity [34–38,41–47]. Foremost among these are indirect interactions between the a and A states mediated by the a', e, d, I, and D states and between the a', e. d, I, and D states mediated by the a

Table 3
Wavenumbers (in cm^{-1}) of the $^{12}C^{18}O$ $B^1\Sigma^+ \rightarrow A^1\Pi(0, 3)$, Vis-FT emission band of $^{12}C^{18}O$.[a,b,c]

J''	$R(J'')$		$Q(J'')$		$P(J'')$	
	σ	$u(\sigma)$	σ	$u(\sigma)$	σ	$u(\sigma)$
1	17,928.68[b]	0.03	17,921.257	0.005	17,917.55[b]	0.02
2	17,933.96[b]	0.01	17,922.822	0.005	17,915.403[b]	0.008
3	17,940.022[b]	0.007	17,925.182	0.005	17,914.050	0.005
4	17,946.873[b]	0.006	17,928.321	0.005	17,913.479	0.005
5	17,954.504	0.005	17,932.247	0.005	17,913.694	0.005
6	17,962.923[b]	0.005	17,936.957	0.005	17,914.696[b]	0.005
7	17,972.123[b]	0.005	17,942.453	0.005	17,916.483	0.005
8	17,982.110	0.005	17,948.734	0.005	17,919.056	0.005
9	17,992.876	0.005	17,955.799	0.005	17,922.417[b]	0.005
10	18,004.432	0.005	17,963.650	0.005	17,926.563	0.005
11	18,016.763	0.005	17,972.287[b]	0.005	17,931.497	0.005
12	18,029.894	0.005	17,981.704	0.005	17,937.219[b]	0.005
13	18,043.807[b]	0.005	17,991.923	0.005	17,943.721[b]	0.005
14	18,058.499	0.005	18,002.930	0.005	17,951.030	0.005
15	18,073.979	0.005	18,014.719[b]	0.005	17,959.128	0.005
16	18,090.239	0.005	18,027.295	0.005	17,968.002	0.005
17	18,107.306	0.005	18,040.694	0.005	17,977.689	0.005
18	18,125.162	0.005	18,054.915	0.005	17,988.172	0.005
19	18,143.826[b]	0.005	18,070.092	0.005	17,999.467	0.005
20	18,163.328	0.005	18,082.720[b]	0.005	18,011.605	0.005
21	18,183.771	0.005	18,101.366	0.005	18,024.692	0.005
22	18,206.004[b]	0.006	18,118.894	0.005	18,039.571	0.005
23	18,224.421	0.005	18,137.101	0.005	18,050.637[b]	0.005
24	18,247.743[b]	0.006	18,156.144	0.005	18,066.627[b]	0.005
25	18,271.271	0.005	18,176.571	0.005	18,082.833[b]	0.005
26	18,295.471[b]	0.006	18,195.242[b]	0.005	18,099.703	0.005
27	18,320.412[b]	0.006	18,216.895	0.005	18,117.332[b]	0.006
28	18,346.129	0.005	18,239.029	0.005	18,135.737	0.005
29	18,372.617	0.005	18,261.904	0.005	18,154.921[b]	0.007
30	18,399.887	0.004	18,285.546	0.005	18,174.909	0.005
31	18,427.942	0.004	18,309.971	0.005	18,195.688[b]	0.007
32	18,456.785	0.004	18,335.188	0.005	18,217.259	0.005
33	18,486.412	0.004	18,361.211	0.005	18,239.646[b]	0.008
34	18,516.733	0.004	18,387.858	0.005	18,262.683	0.006
35	18,548.005[b]	0.004	18,415.555	0.006	18,286.696	0.007
36	18,580.032	0.004	18,443.950	0.006	18,311.507	0.008
37	18,612.82[b]	0.03	18,473.152	0.006	18,337.08[b]	0.02
38	18,646.42[b,w]	0.08	18,503.144	0.007	18,363.47[b]	0.02
39			18,533.956	0.008	18,390.65	0.02
40			18,565.60[b,w]	0.05	18,418.66[b]	0.03

[a] The instrumental resolution was 0.018 cm^{-1}. The estimated absolute calibration uncertainty was 0.004 cm^{-1}. The absolute accuracy of the wavenumber measurements was estimated to be 0.005 cm^{-1}.

[b] The lines marked *b* and/or *w* are blended, and/or weak (SNR < 3).

[c] One standard deviation $u(\sigma)$ represents combinations of the calibration and fitting errors of the wavenumber measurements.

Table 4
Wavenumbers (in cm^{-1}) of the $C^1\Sigma^+ \rightarrow A^1\Pi(0, 3)$, Vis-FT emission band of $^{12}C^{18}O$.[a,b,c]

J''	$R(J'')$		$Q(J'')$		$P(J'')$	
	σ	$u(\sigma)$[c]	σ	$u(\sigma)$[c]	σ	$u(\sigma)$[c]
1			22,923.37[b,w]	0.05		
2			22,924.96[b,w]	0.03	22,917.53[b,w]	0.04
3	22,942.07	0.02	22,927.27[b]	0.02	22,916.17	0.02
4	22,948.89[b]	0.03	22,930.378	0.007	22,915.58[b]	0.02
5	22,956.48	0.01	22,934.266	0.007	22,915.74[b]	0.03
6	22,964.84	0.01	22,938.928[b]	0.009	22,916.708	0.009
7	22,973.98[b]	0.02	22,944.368	0.006	22,918.45[b]	0.02
8	22,983.894	0.008	22,950.585	0.005	22,920.970	0.007
9	22,994.589	0.008	22,957.580	0.005	22,924.268	0.006
10	23,006.06[b]	0.02	22,965.351[b]	0.007	22,928.348	0.006
11	23,018.30[b]	0.02	22,973.907[b]	0.007	22,933.202	0.006
12	23,031.32[b]	0.02	22,983.237[b]	0.006	22,938.834[b]	0.009
13	23,045.12[b]	0.02	22,993.350	0.005	22,945.254	0.006
14	23,059.703	0.008	23,004.243	0.005	22,952.462[b]	0.008
15	23,075.059	0.008	23,015.921	0.005	22,960.443	0.006
16	23,091.198	0.008	23,028.378	0.005	22,969.202	0.006
17	23,108.131	0.008	23,041.650	0.005	22,978.772	0.006
18	23,125.843	0.009	23,055.740	0.005	22,989.13[b]	0.01
19	23,144.366	0.009	23,070.774	0.006	23,000.287	0.007
20	23,163.72[b]	0.02	23,083.259	0.007	23,012.291	0.007
21	23,184.01	0.01	23,101.754	0.006	23,025.230	0.007
22	23,206.07[b]	0.03	23,119.127	0.006	23,039.959	0.008
23	23,224.32[b]	0.03	23,137.169[b]	0.009	23,050.872	0.008
24	23,247.47[b]	0.03	23,156.04[b]	0.02	23,066.70[b]	0.02
25	23,270.83[bw]	0.03	23,176.29[b]	0.02	23,082.730	0.008
26	23,294.85[bw]	0.03	23,194.802	0.007	23,099.44[b]	0.02
27	23,319.60[w]	0.02	23,216.273	0.009	23,116.87[b]	0.02
28	23,345.13[bw]	0.05	23,238.24[b]	0.02	23,135.11[b,w]	0.03
29	23,371.43[w]	0.03	23,260.90[b]	0.04	23,154.12[w]	0.02
30	23,398.515[w]	0.004	23,284.36[b]	0.03	23,173.92[b,w]	0.04
31	23,426.367[b,w]	0.004	23,308.60[b]	0.03	23,194.51[b,w]	0.03
32			23,333.62[w]	0.02	23,215.88[w]	0.03
33			23,359.45[w]	0.02	23,238.08[b,w]	0.03
34			23,385.93[w]	0.03	23,260.90[b,w]	0.07

[a] The instrumental resolution was 0.018 cm^{-1}. The estimated absolute calibration uncertainty was 0.004 cm^{-1}. The absolute accuracy of the line frequency measurements was estimated to be 0.007 cm^{-1}.

[b] The lines marked *b* and/or *w* are blended, and/or weak (SNR < 3).

[c] One standard deviation $u(\sigma)$ represents combinations of the calibration and fitting errors of the wavenumber measurements.

and A states. All of the direct interaction vibrational factors for all of the *intra*-configuration interactions are prohibitively small, as expected for $\Delta v \neq 0$ interactions between states that belong to the same electronic configuration. Almost all of the interaction matrix elements for the *inter*-configuration interactions have been known for many years [33,57,59,61,66,73–75]. This sets the stage for the present results for observations of, among others, indirect *intra*-configurational interactions in CO mediated by known direct *inter*-configurational interactions.

The current deperturbation analysis revealed 2 well determined indirect perturbations, i.e. $A^1\Pi(=3) \sim e^3\Sigma^-(v = 6) \sim a^3\Pi(v = 14)$, where $e^3\Sigma^-(v = 6)$ is an mediating level at $J = 46$–47 as well as $a'^3\Sigma^+(v = 14) \sim A^1\Pi(v = 3) \sim e^3\Sigma^-(v = 6)$, where $A^1\Pi(v = 3)$ mediates the interaction between a' and e states for $J = 50$–53. Both of these cases are discussed below.

As for the direct s-o interaction between $A^1\Pi(v = 3)$ and $a^3\Pi(v = 14)$, it is formally allowed, nevertheless, because of the small value of the vibrational overlap integral, $\langle v_{A(v=3)} | v_{a(v=14)} \rangle_{^{12}C^{18}O} = 9.5 \bullet 10^{-5}$, it could not be observed within the current accuracy of measurements. The significant mixing of the $A^1\Pi(v = 3)$ and $a^3\Pi(v = 14)$ characters, which one can see in Fig. 5 (sub-figures III-IV and VII-VIII), arises because of the presence of the $e^3\Sigma^-(v = 6, F_{1e}, |\Omega| = 1)$ level which lies close to the $a^3\Pi(v = 14, F_{1e}, |\Omega| = 0)$ - $A^1\Pi(v = 3, F_{1e}, |\Omega| = 1)$ diabatic intersection at $J = 46$–47 as well as due to the strong $e^3\Sigma^-(v = 6) \sim A^1\Pi(v = 3)$ and $e^3\Sigma^-(v = 6) \sim a^3\Pi(v = 14)$ direct perturbations (for details see Table 6, Table 7, Fig. 5, Fig. 6. It is best visualised in Fig. 5 (inset III) where at $J = 46$ an admixture of the $A^1\Pi(v = 3, F_{1e}, |\Omega| = 1)$ character is: 9 % for $e^3\Sigma^-(v = 6, F_{1e}, |\Omega| = 1)$ and 3 % for $a^3\Pi(v = 14, F_{1e}, |\Omega| = 0)$. The main role in the $A^1\Pi(v = 3) \sim e^3\Sigma^-(v = 6) \sim a^3\Pi(v = 14)$ intermediate perturbation is played by the homogeneous ($\Delta|\Omega| = 0$) interactions of the spin–orbit nature.

Similarly, the $a'^3\Sigma^+(v = 14)$ and $e^3\Sigma^-(v = 6)$ levels, the spin components of which intersect diabatically for $J = 50$–53, cannot interact directly due to a too-small value of the vibrational overlap integral$\langle v_{a'(v=14)} | v_{e(v=6)} \rangle_{^{12}C^{18}O} = 1.2 \bullet 10^{-3}$. In this case, the $A(v = 3)$ level, which interacts strongly in the specified region of J with both of these levels (for details see Table 6, Table 7, Fig. 5, Fig. 6, mediates a partial exchange of characters between the $a'^3\Sigma^+(v = 14)$ and $e^3\Sigma^-(v = 6)$

Table 5

Wavenumbers (in cm^{-1}) of the interaction-induced lines observed in the $B^1\Sigma^+ \rightarrow A^1\Pi(0, 3)$ and $C^1\Sigma^+ \rightarrow A^1\Pi(0, 3)$, Vis-FT emission bands of $^{12}C^{18}O$.[a,b,c,d]

N	$^rR_{12ee}$		$^rQ_{11ef}$		$^pP_{11ee}$		$^pP_{12ee}$	
J''	σ	$u(\sigma)$	σ	$u(\sigma)$	σ	$u(\sigma)$	σ	$u(\sigma)$
$B^1\Sigma^+$ - $a'^3\Sigma^+(0, 13)$								
20			18,088.745	0.005				
21			18,121.75	0.05				
22	18,195.27^b	0.02					18,028.84^b	0.02
23	18,238.46^b	0.04					18,064.67^w	0.02
$B^1\Sigma^+$ - $D^1\Delta(0, 4)$								
32					18,181.06^b	0.01		
$C^1\Sigma^+$ - $a'^3\Sigma^+(0, 13)$								
20			23,089.28^b	0.02				
…								
22	23,195.35^{b,w}	0.06					23,029.23^w	0.02

[a] The instrumental resolution was 0.018 cm^{-1}. The estimated absolute calibration uncertainty was 0.004 cm^{-1}. The absolute accuracy of the line frequency measurements was estimated to be 0.007 cm^{-1}.

[b] The lines marked *b* and/or *w* are blended, and/or weak (SNR < 3).

[c] The superscripts *p* and *r* denote change in the total angular momentum excluding spin.

[d] One standard deviation $u(\sigma)$ represents combinations of the calibration and fitting errors of the wavenumber measurements.

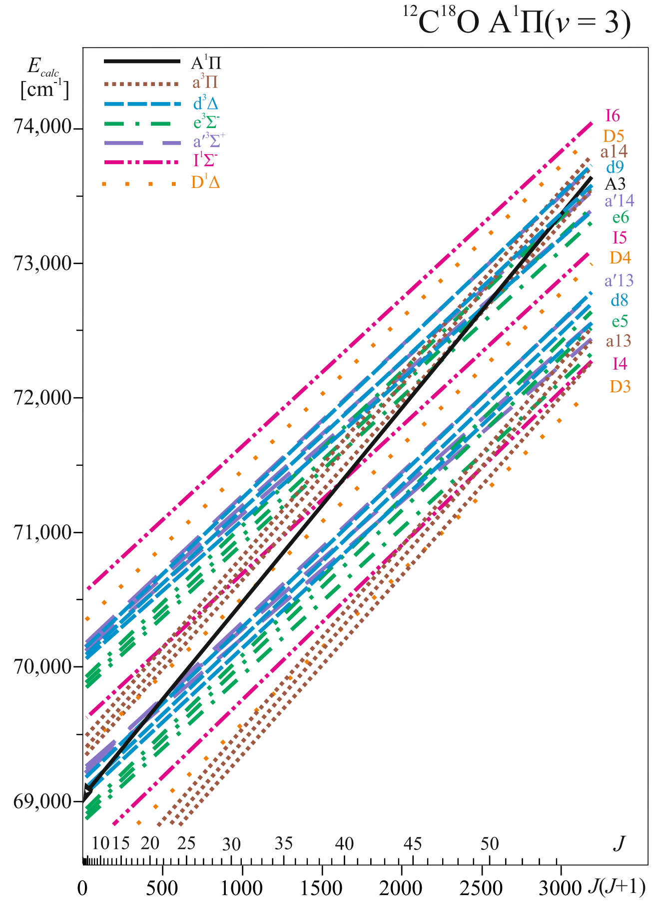

Fig. 4. Ro-vibronic term series in the energy neighbourhood of the $A^1\Pi(v = 3)$ level in the 69,000–74,000 cm^{-1} spectral region of the $^{12}C^{18}O$ isotopologue.

levels. It is most visible in Fig. 6: *(i)* (inset III) where at $J = 53$ an admixture of the $e^3\Sigma^-(v = 6, F_{3e}, |\Omega| = 0)$ character is: 19 % for $A^1\Pi(v = 3, F_{1e}, |\Omega| = 1)$ and 2 % for $a'^3\Sigma^+(v = 14, F_{2e}, |\Omega| = 1)$; *(ii)* (inset VIII) where at $J = 50$ an admixture of the $a'^3\Sigma^+(v = 14, F_{1f}, |\Omega| = 1)$ character is: 27 % for $A^1\Pi(v = 3, F_{1f}, |\Omega| = 1)$ and 3 % for $e^3\Sigma^-(v = 6, F_{2f}, |\Omega| = 1)$.

The vibrational overlap integrals of the direct perturbation matrix elements, verified during the deperturbation analysis of the $A^1\Pi(v = 3)$ level, are listed in Table 6. They have been computed from RKR potential energy curves based on isotopically recalculated equilibrium constants of Field [57], Field et al. [33,73], Le Floch et al. [59], and Kittrell et al. [61].

4. Discussion

The $B^1\Sigma^+$ - $A^1\Pi(0, 3)$ and $C^1\Sigma^+$ - $A^1\Pi(0, 3)$ bands of the $^{12}C^{18}O$ isotopologue had been studied several times [78,79] up to $J_{max} = 39$, with the highest accuracy up to 0.07 cm^{-1} for $B^1\Sigma^+$ - $A^1\Pi(0, 3)$ [78]. The $A^1\Pi$ - $X^1\Sigma^+(3, 0)$ band of $^{12}C^{18}O$ was investigated in Refs. [40,80–82] up to $J_{max} = 22$ and with the highest accuracy of $\sim$ 0.05 cm^{-1} [40].The high-resolution measurements conducted in the framework of the current investigation have been done using modern Fourier-transform spectroscopy techniques with an accuracy of: *(i)* 0.005 cm^{-1} for B - A (0, 3) up to $J_{max} = 40$, *(ii)* 0.007 cm^{-1} for C - A(0, 3) up to $J_{max} = 34$, and *(iii)* 0.03 cm^{-1} for A - X(3, 0) up to $J_{max} = 54$. In addition, a significantly larger number of extra-lines, originating from the perturber level under consideration, are observed in the current work compared to the previous ones [40]. Moreover, the precision of the $A^1\Pi(v = 3)$ term values determined in this work (see Table 8 is measured a factor of 10 times better compared to the best previous investigation ([40], Table 1).

The first and so far the only deperturbation analysis of the $A^1\Pi(v = 3)$ level in $^{12}C^{18}O$ was carried out by Beaty et al. [40] taking into account only 4 fixed in the fit interaction parameters, i.e $A^1\Pi(v = 3) \sim [e^3\Sigma^-(v = 5)$, $d^3\Delta(v = 8)$, $a'^3\Sigma^+(v = 13)$ and $D^1\Delta(v = 4)]$. In this work, 9 interactions, of which 4 were fitted, proved to be significant within the accuracy of the line position measurements, and were taken into account. They contained the 3 above-mentioned interactions, in addition to $A^1\Pi(v = 3) \sim d^3\Delta(v = 8)$, as well as newly-modelled: *(i)* direct $A^1\Pi(v = 3) \sim [a'^3\Sigma^+(v = 14)$, $d^3\Delta(v = 9)$, $e^3\Sigma^-(v = 6)]$ spin–orbit interactions and the $A^1\Pi(v = 3) \sim I^1\Sigma^-(v = 5)$ $\boldsymbol{L}$-uncoupling ones; *(ii)* indirect $a^3\Pi(v = 14) \sim e^3\Sigma^-(v = 6) \sim A^1\Pi(v = 3)$ interaction, where the $e^3\Sigma^-(v = 6)$ is the mediating level and the $a^3\Pi(v = 14) \sim e^3\Sigma^-(v = 6)$ perturbation manifests the combined, spin–orbit, spin-electronic and rotation-electronic nature; *(iii)* an indirect $a'^3\Sigma^+(v = 14) \sim A^1\Pi(v = 3) \sim e^3\Sigma^-(v = 6)$ interaction with the spin–orbit natures, where the $A^1\Pi(v = 3)$ level acts as an mediating level (see Table 6 and Table 7 for details). The $A^1\Pi(v = 3) \sim d^3\Delta(v = 8)$ spin–orbit perturbation turns out to be too weak to be observed even within the current, 10 times higher than in the literature, accuracy of measurements. This is due to the small vibrational overlap integral which is $\langle v_{A(v=3)}|v_{d(v=8)}\rangle = 6.0 \bullet 10^{-3}$.

Fig. 7 presents reduced term values of $^{12}C^{18}O$ $A^1\Pi(v = 3)$, calculated based on the current experimental data. The largest level shifts occur at the anti-crossing of the: *(i)* $A^1\Pi(v = 3, F_{1f})$ and $a'^3\Sigma^+(v = 13, F_{1f})$ at $J = 20$ (approx. 2.5 cm^{-1}); *(ii)* $A^1\Pi(v = 3, F_{1f})$ and $[e^3\Sigma^-(v = 6, F_{2f})$, $a'^3\Sigma^+(v$

Table 6
Verification of the unimolecular interactions during the deperturbation analysis of the $A^1\Pi(v=3)$ level of $^{12}C^{18}O$.

Nº	Interactions			Nature of the perturbation	$\langle v_i \vert v_j \rangle$ [a] or $\langle v_i \vert \boldsymbol{B}(\boldsymbol{R}) \vert v_j \rangle$ [b]	Included into the final fit	Status	Notes[c]
1	$A^1\Pi(v=3)$	~	$e^3\Sigma^-(v=4)$	Spin-orbit	0.028[a]	No	-	Irrelevant.
2	“	~	$e^3\Sigma^-(v=5)$	“	−0.204[a]	Yes	Fixed	Noticeable. Floating causes correlation with the T of A(3) and divergency of the fit.
3	“	~	$e^3\Sigma^-(v=6)$	“	0.261[a]	Yes	Floated	–
4	“	~	$e^3\Sigma^-(v=7)$	“	−0.223[a]	No	–	Irrelevant.
5	“	~	$d^3\Delta(v=7)$	“	−0.133[a]	No	–	Irrelevant.
6	“	~	$d^3\Delta(v=8)$	“	0.007[a]	No	–	Irrelevant.*
7	“	~	$d^3\Delta(v=9)$	“	0.100[a]	Yes	Fixed	Noticeable. Floating causes divergency of the fit.
8	“	~	$d^3\Delta(v=10)$	“	−0.176[a]	No	–	Irrelevant.
9	“	~	$a'^3\Sigma^+(v=12)$	“	−0.226[a]	No	–	Irrelevant.
10	“	~	$a'^3\Sigma^+(v=13)$	“	0.198[a]	Yes	Floated	–
11	“	~	$a'^3\Sigma^+(v=14)$	“	−0.168[a]	Yes	Fixed	Noticeable. Floating causes divergency of the fit.
12	“	~	$a'^3\Sigma^+(v=15)$	“	0.139[a]	No	–	Irrelevant.
13	“	~	$D^1\Delta(v=2)$	*L*-uncoupling	−0.367[b]	No	–	Irrelevant.
14	“	~	$D^1\Delta(v=3)$	“	0.386[b]	No	–	Irrelevant.
15	“	~	$D^1\Delta(v=4)$	“	−0.160[b]	Yes	Floated	–
16	“	~	$I^1\Sigma^-(v=4)$	“	−0.074[b]	No	–	Irrelevant.
17	“	~	$I^1\Sigma^-(v=5)$	“	−0.193[b]	Yes	Floated	–
18	“	~	$I^1\Sigma^-(v=6)$	“	0.340[b]	No	–	Irrelevant.
19	$d^3\Delta(v=8)$	~	$e^3\Sigma^-(v=5)$	Spin-spin	0.010[a]	No	–	Irrelevant.
20	“	~	$a'^3\Sigma^+(v=13)$	“	$7.5\bullet10^{-4}$ [a]	No	–	Irrelevant.*
21	$d^3\Delta(v=9)$	~	$e^3\Sigma^-(v=6)$	“	0.011[a]	No	–	Irrelevant.
22	“	~	$a'^3\Sigma^+(v=14)$	“	$7.8\bullet10^{-4}$ [a]	No	–	Irrelevant.*
23	$e^3\Sigma^-(v=6)$	~	“	Spin-orbit	−0.001[a]	No	–	Irrelevant.*
24	$a^3\Pi(v=13)$	~	$d^3\Delta(v=8)$	Spin-orbit/spin-electronic.	−0.201[a]	No	–	Irrelevant.
25	“	~	“	*L*-uncoupling.	−0.210[b]	No	–	Irrelevant.
26	“	~	$a'^3\Sigma^+(v=13)$	Spin-orbit/spin-electronic.	0.204[a]	No	–	Irrelevant.
27	“	~	“	*L*-uncoupling.	0.249[b]	No	–	Irrelevant.
28	“	~	$e^3\Sigma^-(v=5)$	Spin-orbit/spin-electronic.	0.317[a]	No	–	Irrelevant.
29	“	~	“	*L*-uncoupling.	0.302[b]	No	–	Irrelevant.
30	$a^3\Pi(v=14)$	~	$A^1\Pi(v=3)$	Spin-orbit	$9.5\bullet10^{-5}$ [a]	No	–	Irrelevant.*
31	“	~	$e^3\Sigma^-(v=6)$	Spin-orbit/spin-electronic.	0.201[a]	Yes	Fixed	Noticeable. Floating causes divergency of the fit.
32	“	~	“	*L*-uncoupling.	0.187[b]	Yes	Fixed	Noticeable. Floating makes the a(14) ~ e(6) spin–orbit/spin-electronic interaction parameter no longer statistically justified.
33	“	~	$d^3\Delta(v=8)$	Spin-orbit/spin-electronic.	−0.263[a]	No	–	Irrelevant.
34	“	~	“	*L*-uncoupling.	−0.264[b]	No	–	Irrelevant.
35	“	~	$d^3\Delta(v=9)$	Spin-orbit/spin-electronic.	−0.088[a]	No	–	Irrelevant.
36	“	~	“	*L*-uncoupling.	−0.091[b]	No	–	Irrelevant.
37	“	~	$a'^3\Sigma^+(v=13)$	Spin-orbit/spin-electronic.	0.033[a]	No	–	Irrelevant.
38	“	~	“	*L*-uncoupling.	0.038[b]	No	–	Irrelevant.
39	“	~	$a'^3\Sigma^+(v=14)$	Spin-orbit/spin-electronic.	0.153[a]	No	–	Irrelevant.
40	“	~	“	*L*-uncoupling.	0.184[b]	No	–	Irrelevant.
41	“	~	$D^1\Delta(v=4)$	Spin-orbit	0.380[a]	No	–	Irrelevant.
42	“	~	$I^1\Sigma^-(v=5)$	“	0.382[a]	No	–	Irrelevant.

[a] The vibrational overlap integrals $\langle v_i \vert v_j \rangle$. They were calculated as it was described in Refs. [34,35].

[b] The rotational operator integrals $\langle v_i \vert \boldsymbol{B}(\boldsymbol{R}) \vert v_j \rangle$ in cm^{-1}. They were calculated as it was described in Refs. [34,35].

[c] Relevance of the parameters was tested in the way described in detail in Ref. [38].

*The value of the vibrational overlap integral is too small in relation to the accuracy of measurements thus the interaction is negligible.

Table 7

Deperturbed molecular parameters of the $A^1\Pi(v = 3)$ level and its perturbers in ${}^{12}C^{18}O$[a,b]

Constant	$A^1\Pi(v = 3)$		$I^1\Sigma^-(v = 5)$	$D^1\Delta(v = 4)$	
	this work	Ref. [40]		this work	Ref. [40]
T_v	68,996.1489(13)	68,997.469(15)	69,588.128(45)	69,391.034(11)	69,392.24
B	1.4636691(55)	1.463549(93)	1.1184[c]	1.1233[f]	1.12330
$q \times 10^5$	–1.34(15)				
$D \times 10^6$	6.9208(73)	6.65	6.30[d]	6.32[f]	6.39
$H \times 10^{12}$	–31.8(26)		2.59[d]	–0.26[d]	
$\xi(A^1\Pi_{v=3} \sim v^{''}) \times 10^2$			–2.830(69)	–2.481(38)	–0.20[g]*
Constant	$e^3\Sigma^-$ $(v = 5)$		$e^3\Sigma^-$ $(v = 6)$		
	this work	Ref. [40]			
T_v	68,879.56[h]	68,879.55	69,856.49[h]		
B	1.1332[c]	1.13316	1.1175[c]		
A					
$A_D \times 10^5$					
$D \times 10^6$	6.04[c]	6.14	6.02[c]		
$H \times 10^{12}$	–1.73[d]		–1.73[d]		
λ	0.60[c]	0.69	0.62[c]		
$\gamma \times 10^2$					
$\eta(A^1\Pi_{v=3} \sim v^{''})$	–8.73[i]	–9.63[g]	11.644(87)		
$\eta(a^3\Pi_{v=14} \sim v^{''})$			12.19[j]		
$\xi(a^3\Pi_{v=14} \sim v^{''}) \times 10^2$			3.0[j]		
Constant	$d^3\Delta(v = 9)$	$a'^3\Sigma^+(v = 13)$		$a'^3\Sigma^+(v = 14)$	$a^3\Pi(v = 14)$
		this work	Ref. [40]		
T_v	70,065.71[h]	69,203.2371(28)	69,203.08	70,139.43[h]	69,378.33[l]
B	1.0987[c]	1.07[c]	1.06871	1.0539[c]	1.3462[c]
A	–17.36[c]				38.09[c]
$A_D \times 10^5$	–9.62[k]				–18.70[m]
o					0.63[n]
$p \times 10^3$					2.64[o]
$q \times 10^5$					2.83[n]
$D \times 10^6$	5.81[c]	5.66[c]	5.81	5.66[c]	6.34[c]
$H \times 10^{12}$	–0.69[d]	–0.35[d]		–0.35[d]	
λ	1.29[c]	–1.1168(91)	–1.15	–1.12[c]	–0.97[m]
$\gamma \times 10^2$	–0.95[k]	–0.49[k]		–0.47[k]	0.30[k]
$\eta(A^1\Pi_{v=3} \sim v^{''})$	5.92[i]	– 7.1819(43)	–7.3[g]	6.06[i]	

[a] Values are given in cm^{-1}. The η and ξ symbols indicate a spin–orbit and rotation-electronic interaction parameter, respectively. Note that the $\eta_{a\sim e,d,a'}$ parameters represent a linear combinations of spin–orbit and spin-electronic interactions, because both of them reveal the same *Ω*-dependence, so they cannot be determined independently.

Note that the data obtained by Beaty et al. [40] were calculated using the $\widehat{\boldsymbol{R}}$ operator, whereas our analysis is based on the $\widehat{N}$ one.

[b] Values in parentheses indicate 1σ uncertainties of parameters floated in the analysis and expressed in units of the least significant digit. All other parameters were fixed during the final deperturbation fit. Molecular constants of the ${}^{12}C^{18}O$ $X(v = 0)$ ground state were fixed to the values determined by Coxon and Hajigeorgiou [58]: $G_v = 1055.7172740$, $B_v = 1.830980706$, $D_v = 5.550179 \times 10^{-6}$, $H_v = 5.01843 \times 10^{-12}$, $L_v = –3.0008 \times 10^{-17}$, $M_v = –3.80 \times 10^{-23}$, $N_v = –6.0 \times 10^{-28}$, and $O_v = –3.0 \times 10^{-33}$ cm^{-1}. During the fit, the term values of $B^1\Sigma^+(v = 0)$ and $C^1\Sigma^+(v = 0)$ were fixed to the values obtained by Malicka et al. [42].

[c] Calculated on the basis of Ref. [57] using mass-scaling dependences.

[d] Calculated in this work on the basis of Ref. [59] by isotopic scaling.

[e] The spin–orbit perturbation parameters were obtained on the basis of the isotopologue-independent $\boldsymbol{a_{a\sim I}}$ [73] and $\boldsymbol{a_{a\sim D}}$ [75] parameters as well as on the $\alpha_{a\sim I}(\boldsymbol{a_{a\sim I}})$ and $\alpha_{a\sim D}(\boldsymbol{a_{a\sim D}})$ dependences [33,73]. The $\eta_{a\sim I}(\alpha_{a\sim I})$ and $\eta_{a\sim D}(\alpha_{a\sim D})$ relationships were derived from symmetrized matrix elements of the $a^3\Pi \sim I^1\Sigma^-$ and $a^3\Pi \sim D^1\Delta$ interactions. The vibrational overlap integrals $\langle v_a | v_{I,D} \rangle$ were calculated as described in Ref. [35].

[f] Obtained by isotopic scaling of the values taken from Ref. [61].

[g] The η and ξ parameters were calculated from α and β constants given in Ref. [40] based on Eqs. (2) - (4) in Ref. [38].
(* It seems that the parameter value ξ $(A^1\Pi_{v=3}$ $D^1\Delta_{v=4})$ has an editorial error in the Ref. [40]; it should be 2.0×10^{-2} cm^{-1}).

[h] Calculated in this work on the basis of Refs. [57,58] and isotopic scaling.

[i] The spin–orbit and rotation-electronic interaction parameters were calculated on the basis of isotopologue-independent $\boldsymbol{a_{A\sim d,e,a'}}$ and $\boldsymbol{b_{A\sim D,I}}$ electronic parameters [34,39] based on the equations (1) - (5) from Ref. [34] and (2) - (4) from Ref. [38]. The vibrational overlap integrals $\langle v_A | v_{a',e,d} \rangle$ and rotational operator integrals $\langle v_A | \boldsymbol{B}(\boldsymbol{R}) | v_{I,D} \rangle$ were calculated as it was described in Refs. [34,35].

[j] The spin–orbit with spin-electronic as well as $\boldsymbol{L}$-uncoupling perturbation parameters were obtained on the basis of the isotopologue-independent $\boldsymbol{a_{a\sim e,d,a'}}$ and $\boldsymbol{b_{a\sim e,d,a'}}$ parameters from Ref. [73] as well as on the $\alpha_{a\sim e,d,a'}(\boldsymbol{a_{a\sim e,d,a'}})$ and $\beta_{a\sim e,d,a'}(\boldsymbol{b_{a\sim e,d,a'}})$ dependences [33,73]. The $\eta_{a\sim e,d,a'}(\alpha_{a\sim e,d,a'})$ and $\xi_{a\sim e,d,a'}(\beta_{a\sim e,d,a'})$ relationships were derived from symmetrized matrix elements of the $a^3\Pi \sim e^3\Sigma^-$, $d^3\Delta$, $a'^3\Sigma^+$ interactions in Ref. [38] as equations (5) – (7). The vibrational overlap integrals $\langle v_a | v_{e,d,a'} \rangle$ and rotational operator integrals $\langle v_a | \boldsymbol{B}(\boldsymbol{R}) | v_{e,d,a'} \rangle$ were calculated as described in Ref. [34,35].

[k] Taken from Ref. [57] (in MHz), then converted into cm^{-1} and isotopically scaled.

[l] Calculated on the basis of Refs. [16,57,58] and isotopically scaled if necessary.

[m] Calculated in this work on the basis of Ref. [74] (in MHz), then converted into cm^{-1} and isotopically scaled. The diagonal spin–spin constant $\lambda = 1.5 \times \varepsilon$.

[n] Calculated in this work based on Ref. [83] ($o = C^{\delta}$ or $q = 2 \times B_{0+}$) by isotopic scaling procedure.

[o] Obtained by isotopic scaling of the values taken from Ref. [74] ($p = 2 \times p_{+}$).

Table 8
Term values (in cm^{-1}) of the $A^1\Pi(v = 3)$ level in $^{12}C^{18}O$.[a,b,c,d]

J	F_{1e} (cm^{-1})	u	$^1\Pi$ (%)	*(obs-calc)/u*	F_{1f} (cm^{-1})	u	$^1\Pi$ (%)	*(obs-calc)/u*
1	68,999.14	0.02	99.77	0.31	68,999.138	0.009	99.77	0.23
2	69,004.991	0.008	99.77	0.41	69,004.993	0.007	99.77	0.81
3	69,013.766	0.006	99.77	0.24	69,013.765	0.007	99.77	0.18
4	69,025.467	0.005	99.78	0.08	69,025.466	0.006	99.78	0.14
5	69,040.093	0.005	99.78	0.04	69,040.091	0.006	99.79	0.03
6	69,057.643	0.005	99.79	0.08	69,057.640	0.006	99.79	−0.01
7	69,078.114	0.005	99.79	−0.24	69,078.112	0.005	99.80	0.01
8	69,101.508	0.004	99.80	−0.25	69,101.505	0.005	99.81	−0.06
9	69,127.822	0.004	99.81	−0.28	69,127.821	0.005	99.81	0.39
10	69,157.055	0.004	99.81	−0.22	69,157.052	0.006	99.81	0.18
11	69,189.206	0.004	99.81	0.10	69,189.200	0.006	99.81	0.03
12	69,224.272	0.004	99.81	0.45	69,224.267	0.006	99.81	0.67
13	69,262.250	0.004	99.81	0.69	69,262.247	0.005	99.80	1.53
14	69,303.135	0.004	99.80	0.25	69,303.126	0.005	99.78	0.60
15	69,346.927	0.004	99.78	−0.11	69,346.915	0.005	99.75	0.67
16	69,393.633	0.004	99.75	2.39	69,393.612	0.005	99.68	2.48
17	69,443.215	0.004	99.70	−0.45	69,443.181	0.005	99.53	1.67
18	69,495.699	0.004	99.60	−0.14	69,495.604	0.005	99.12	0.02
19	69,551.054	0.004	99.41	−0.91	69,550.768	0.006	97.02	0.52
20	69,609.255	0.004	98.94	−1.06	69,612.16	0.02	56.65	−2.06
21	69,670.192	0.004	97.24	−0.75	69,671.223	0.006	97.58	−0.72
22	69,733.017	0.005	81.75	−2.54	69,735.071	0.006	99.12	−0.38
23	69,803.328	0.005	90.23	−0.26	69,801.920	0.006	99.22	−0.44
24	69,872.395	0.005	98.17	0.45	69,871.604	0.006	98.46	−1.16
25	69,944.918	0.005	99.28	0.14	69,943.568	0.006	87.49	−2.84
26	70,020.434	0.005	99.62	0.23	70,020.946	0.007	94.85	2.54
27	70,098.859	0.006	99.76	−0.04	70,099.010	0.007	99.08	1.15
28	70,180.168	0.005	99.83	−0.26	70,180.240	0.007	99.61	0.29
29	70,264.350	0.006	99.87	0.14	70,264.392	0.007	99.77	0.24
30	70,351.386	0.005	99.89	−0.65	70,351.422	0.007	99.84	0.63
31	70,441.279	0.005	99.90	−0.37	70,441.302	0.008	99.87	−0.05
32	70,534.016	0.006	99.87	0.14	70,534.035	0.008	99.86	0.31
33	70,629.578	0.007	99.57	1.87	70,629.591	0.008	99.56	1.41
34	70,728.120	0.007	99.10	1.66	70,728.132	0.009	99.09	1.09
35	70,829.296	0.007	99.87	−0.14	70,829.30	0.01	99.86	−1.06
36	70,933.342	0.007	99.91	−1.33	70,933.35	0.02	99.90	−0.69
37	71,040.22	0.02	99.92	−0.38	71,040.22	0.02	99.90	−0.89
38	71,149.90	0.02	99.92	−0.60	71,149.90	0.02	99.89	−0.62
39	71,262.40	0.02	99.91	0.54	71,262.37	0.02	99.84	−0.78
40	71,377.67	0.02	99.90	0.06	71,377.60	0.03	99.58	−0.42
41	71,495.73	0.03	99.88	0.09	71,497.24	0.04	55.37	−0.61
42	71,616.56	0.03	99.84	0.04	71,616.70	0.04	99.55	−0.43
43	71,740.16	0.03	99.77	0.49	71,740.28	0.04	99.78	0.04
44	71,866.47	0.03	99.60	0.20	71,866.62	0.04	99.78	−0.26
45	71,995.42	0.03	98.96	−0.41	71,995.74	0.04	99.72	0.29
46	–	–	–	–	72,127.56	0.05	99.44	0.37
47	72,263.73	0.04	92.59	1.62	72,262.08	0.05	99.18	0.37
48	72,400.26	0.05	99.02	1.17	72,399.14	0.07	98.26	0.60
49	72,540.09	0.06	99.46	−0.13	72,537.81	0.06	90.38	−0.94
50	72,682.80	0.07	99.33	0.82	–		–	–
51	–		–	–	72,829.68	0.09	95.79	−0.39
52	–		–	–	72,977.37	0.09	99.09	0.22
53	–		–	–	73,128.0	0.5	99.13	−0.01
54	–		–	–	73,282.8	0.2	77.90	0.27
55	73,438.21	0.07	99.12	−0.43				

[a] All term values are given in cm^{-1} in relation to the $X(v = 0, J = 0)$ level.
[b] Calculated based on $^{12}C^{18}O$ A - X(3, 0), B - A(0, 3) and C - A(0, 3) transition energies and $^{12}C^{18}O$ B(0), C(0) term values given by Malicka et al. [42].
[c] $^1\Pi$ (%) fractional character of $A^1\Pi(v = 3)$.
[d] One standard deviation u indicate the random (fitting) errors of the terms.

$= 14, F_{1f})]$ at $J = 49$ (ca. 2.3 cm^{-1}); *(iii)* $A^1\Pi(v = 3, F_{1e})$ and $a'^3\Sigma^+(v = 13, F_{2e})$ at $J = 22$ (approx. 2.0 cm^{-1}); *(iv)* $A^1\Pi(v = 3, F_{1e})$ and $d^3\Delta(v = 9, F_{1e})$ at $J = 54$ (about 1.9 cm^{-1}) that are the result of the spin–orbit perturbations; *(v)* $A^1\Pi(v = 3, F_{1f})$ and $I^1\Sigma^-(v = 5, F_{1f})$ at $J = 41$ (ca. 1.3 cm^{-1}) as a result of a rotation-electronic ($\boldsymbol{L}$-uncoupling) perturbation. One of the smallest reduced level shifts visible in Fig. 7 is caused by the direct rotation-electronic perturbation of the $A^1\Pi(v = 3, F_{1ef})$ and $D^1\Delta(v = 4, F_{1ef})$ levels at $J = 34$ (ca. 0.1 cm^{-1}). This is caused by the relatively small value of the rotational operator integral $\langle \upsilon_{A(3)} | \boldsymbol{B}(\boldsymbol{R}) | \upsilon_{D(4)} \rangle = 0.1534$ cm^{-1} and the large energy separation (about 9.3 cm^{-1}) between the diabatic $A^1\Pi(v = 3)$ and $D^1\Delta(v = 4)$ levels. It should be noted that, based on the experimental data, we were unable to determine the term values of $A^1\Pi(v = 3, F_{1e})$ for $J = 46$, 51, 53 and $A^1\Pi(v = 3, F_{1f})$ for $J = 50$ (see Table 9) because of the rapid decrease of the intensities of the spectral lines. The weaknesses are caused by the direct $A^1\Pi(v = 3) \sim e^3\Sigma^-(v = 6)$ and indirect $a^3\Pi(v = 14) \sim e^3\Sigma^-(v = 6) \sim A^1\Pi(v = 3)$ perturbations at $J = 46$–47 and by the multi-state $A^1\Pi(v = 3) \sim [e^3\Sigma^-(v = 6), a'^3\Sigma^+(v = 14)]$ perturbations at $J = 50$ and 52–53 for the *f*- and *e*-symmetry levels, respectively. Therefore, the information on the magnitude of these term shifts is less reliable; therefore only predicted, theoretical values of them were calculated, i.e. 1.6, 0.3, and 2.9 cm^{-1} for $J = 46$, 51, 53 of $A^1\Pi(v =$

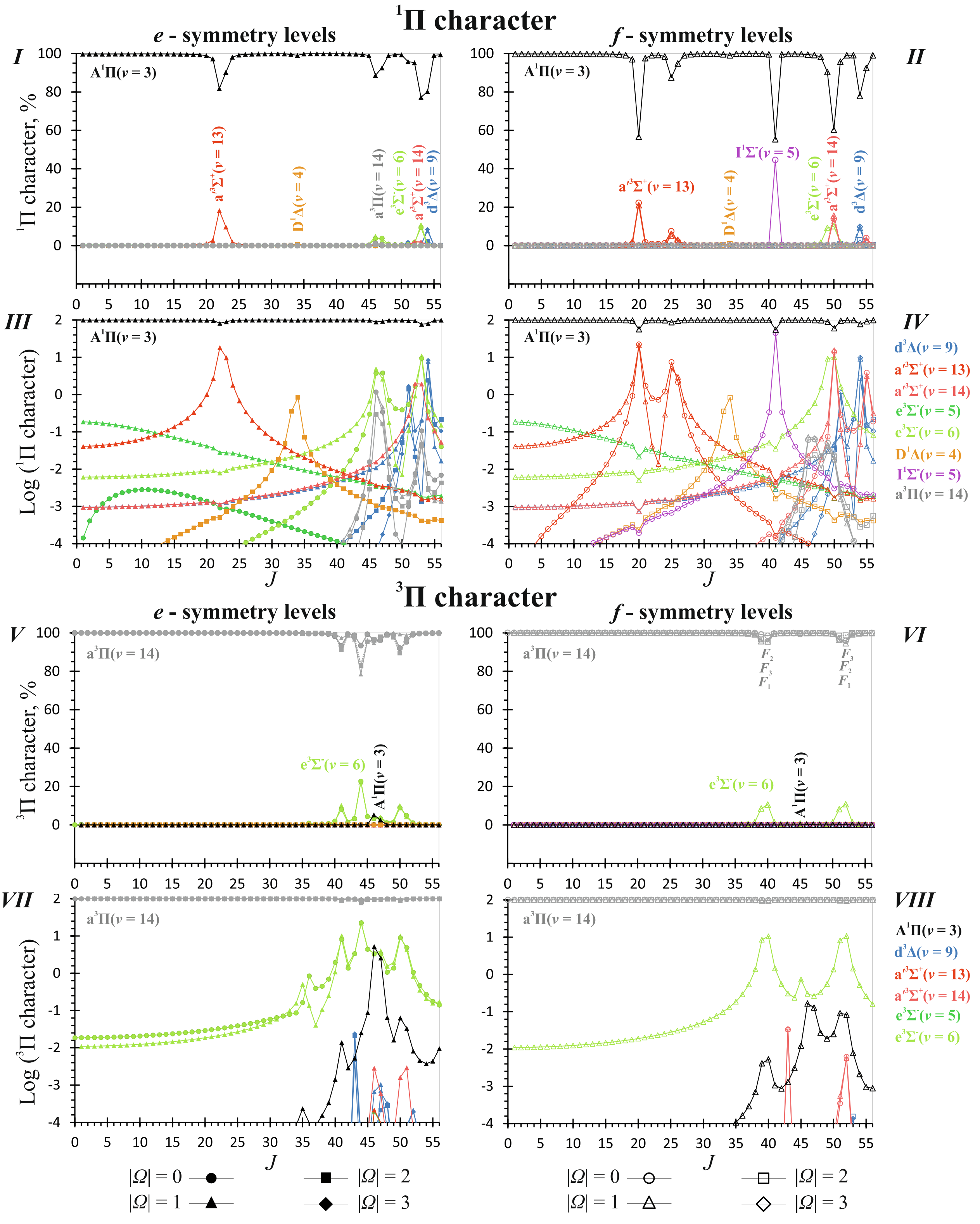

Fig. 5. Fractional $^1\Pi$ (sub-figures I-IV) and $^3\Pi$ (sub-figures V-VIII) characters of the ro-vibronic levels involved in the perturbations of the $^{12}C^{18}O$ A$^1\Pi(v = 3)$ and a$^3\Pi(v = 14)$ levels as well as their perturbers within the observational spectral range.

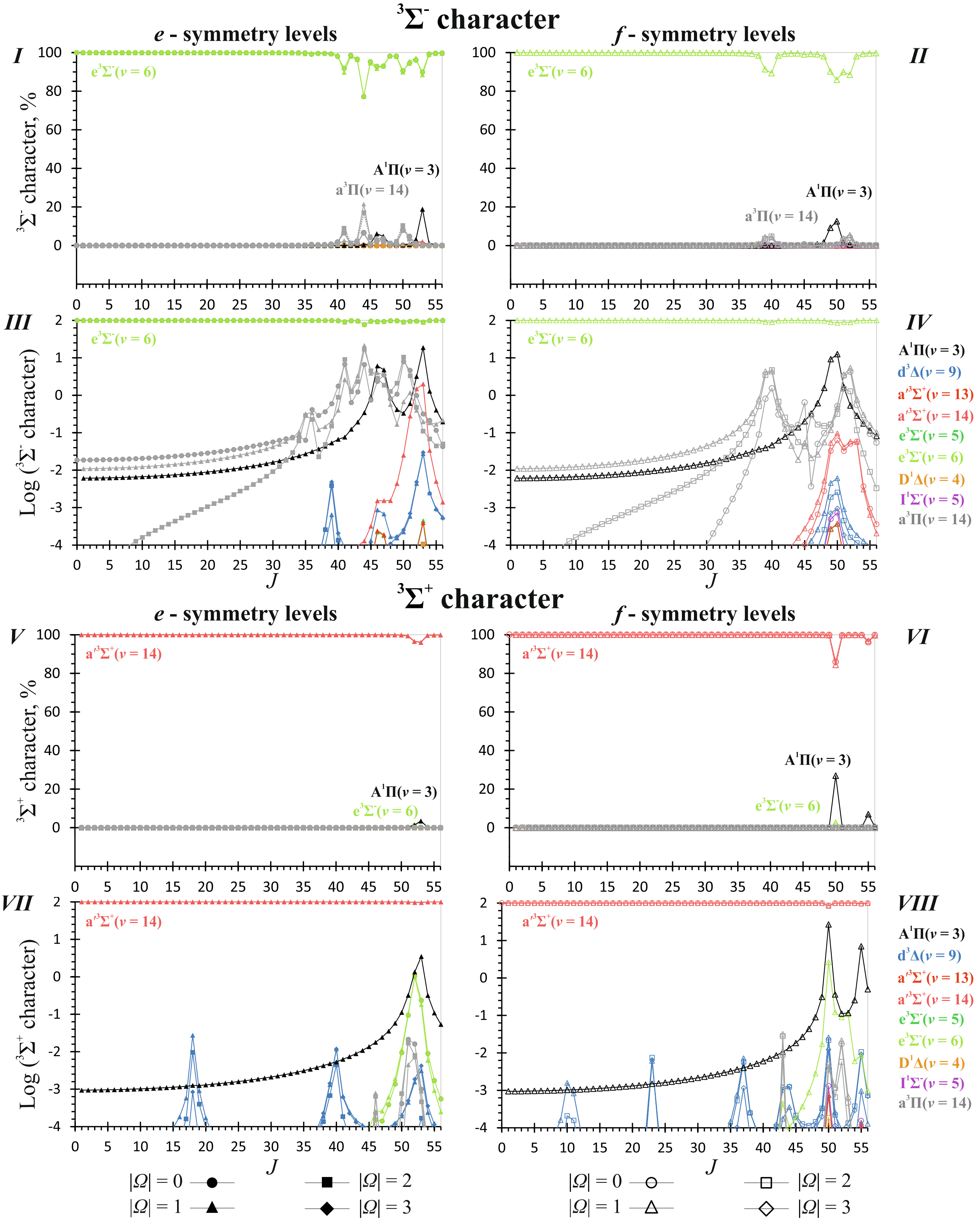

Fig. 6. Fractional $^3\Sigma^-$ (sub-figures I-IV) and $^3\Sigma^+$ (sub-figures V-VIII) characters of the ro-vibronic levels involved in the perturbations of the $^{12}C^{18}O$ $A^1\Pi(v = 3)$ and $a^3\Pi(v = 14)$ levels as well as their perturbers within the observational spectral range.

Table 9

Term values (in cm^{-1}) of perturbers of the A$^1\Pi(v = 3)$ level in ^{12}C^{18}O.[a,b,c,d]

J	a'$^3\Sigma^+$ ($v = 13$)											
	F_{1f} (cm^{-1})	u	$^1\Pi$ (%)	*(obs-calc)/u*	F_{2e} (cm^{-1})	u	$^1\Pi$ (%)	*(obs-calc)/u*	F_{3f} (cm^{-1})	u	$^1\Pi$ (%)	*(obs-calc)/u*
19	69,568.84	0.04	2.01	0.32								
20	69,606.137	0.007	21.10	−1.46	69,650.77	0.04	1.01	−0.26				
21	69,650.89	0.03	0.65	0.42	69,695.69	0.03	2.71	−1.42				
22					69,743.75	0.01	18.21	−2.35				
23					69,789.30	0.03	9.73	−1.29				
…												
26									70,007.82	0.04	2.13	−0.14
27									70,067.57	0.06	0.27	−0.01
J	D$^1\Delta$($v = 4$)								I$^1\Sigma^-$($v = 5$)			
	F_{1e} (cm^{-1})	u	$^1\Pi$ (%)	*(obs-calc)/u*					F_{1f} (cm^{-1})	u	$^1\Pi$ (%)	*(obs-calc)/u*
32	70,570.21	0.02	0.05	−0.32								
…												
41									71,493.92	0.04	44.6	−0.13

[a] All term values are given in cm^{-1} in relation to the X($v = 0$, $J = 0$) level.

[b] Calculated based on ^{12}C^{18}O B(0), C(0) term values given by Malicka et al. and extra-lines [42].

[c] $^1\Pi$ (%) fractional character of A$^1\Pi(v = 3)$.[d] One standard deviation u indicate the random (fitting) errors of the terms.

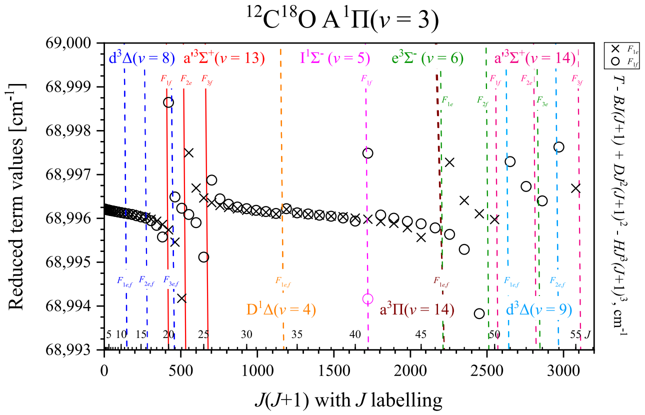

Fig. 7. Ro-vibronic reduced term values of the A$^1\Pi(v = 3)$ level and its perturbers of ^{12}C^{18}O as function of the rotational quantum number J and $J(J + 1)$. The energies are calculated as $[T(J) - BJ(J + 1) + DJ^2(J + 1)^2 - HJ^3(J + 1)^3]$, where the deperturbed T, B, D, and H values of the levels under consideration were taken from the final fit (see Table 7). The A$^1\Pi(v = 3)$ terms were derived based on the experimental transition frequencies. The colourful lines represent the ro-vibronic terms of the perturbers: *(i)* obtained from the current experimental data (solid lines); *(ii)* calculated based on the literature data and using isotopic scaling (dotted lines); see Table 7 for details.

3, F_{1e}), respectively, and 0.9 cm^{-1} for $J = 50$ of A$^1\Pi(v = 3, F_{1f})$.

The $^1\Pi$ fractional character of the perturbed A$^1\Pi(v = 3, F_1, |\Omega| = 1)$ e - and f - Λ – doublet components, is presented in Fig. 5 (sub-figures I-IV) and Table 8. The decrease of their $^1\Pi$ character is caused by interactions with the perturbing states, i.e.: a'$^3\Sigma^+(v = 13, 14)$, D$^1\Delta(v = 4)$, I$^1\Sigma^-(v = 5)$, e$^3\Sigma^-(v = 6)$ and d$^3\Delta(v = 9)$. The largest reduction of the $^1\Pi$ character of the A$^1\Pi(v = 3)$ level, reduced to 56.7 % and 55.4 %, occurs for its F_{1f} component and is mainly caused by the interactions with a'$^3\Sigma^+(v = 13)$ at $J = 20$ and I$^1\Sigma^-(v = 5)$ at $J = 41$, respectively. The largest borrowing of $^1\Pi$ character (44.6 % of $^1\Pi$ at $J = 41$) is made by the F_{1f} component of I$^1\Sigma^-(v = 5)$ and this is due to the direct, but relatively weak heterogeneous rotation-electronic interaction, which notwithstanding, strongly depends on the quantum number J, which plays the key role in this particular case. A much smaller, but still relatively very large admixture of the $^1\Pi$ character occurs for the F_{1f}, F_{2e} and F_{3f} components of the a'$^3\Sigma^+(v = 13)$ level (22.3 % at $J = 20$, 18.2 % at $J = 22$ and 21.1 % at $J = 20$, respectively). The a'$^3\Sigma^+(v = 13)$ level borrows significant $^1\Pi$ character also at $J = 25$ by the F_{1f} and F_{3f} components: 5.0 % and 7.5 %, respectively. Within this work, the transitions associated with the rotational levels up to $J_{max} = 54$ were observed, thus it became possible to analyse interactions within the much higher J 's of A$^1\Pi(v = 3)$ than previously observed, i.e. with: *(i)* e$^3\Sigma^-(v = 6)$ for F_{1e} and F_{3e} at $J = 53$ (theoretical values: 10.9 % and 9.4 % of $^1\Pi$, respectively) and for F_{2f} at $J = 50$ (theoretical value 10.1 % of $^1\Pi$); *(ii)* a'$^3\Sigma^+(v = 14)$ for F_{1f} and F_{3f} at $J = 50$ (theoretical values: 15.5 % and 14.0 % of $^1\Pi$, respectively) and for F_{2e} at $J = 52$ (1.9 % of $^1\Pi$); *iii)* d$^3\Delta(v = 9)$ for all components at $J = 54$ (2.4–7.8 % of $^1\Pi$).

5. Conclusion

The current investigations are based on a large set of high precision experimental data from the combination of modern, high-accuracy VUV-FTS and Vis-FT spectroscopy techniques. Our deperturbation analysis of the A$^1\Pi(v = 3)$ state in the ^{12}C^{18}O isotopologue, based on 571 high precision spectral lines, significantly extends the previous results concerning this state. The maximum rotational quantum number of the analysed rotational levels of A$^1\Pi(v = 3)$ has been increased from previously known $J_{max} = 39$ up to the current $J_{max} = 54$. A significantly larger number of extra-lines originating from perturbations of A$^1\Pi(v = 3)$ were also observed. Finally, 13 parameters were fitted: 9 deperturbed molecular constants of the A$^1\Pi(v = 3)$, a'$^3\Sigma^+(v = 13)$, D$^1\Delta(v = 4)$ and I$^1\Sigma^-(v = 5)$ levels; 2 spin–orbit interaction parameters of the A$^1\Pi(v = 3)$ ~ [e$^3\Sigma^-(v = 6)$, a'$^3\Sigma^+(v = 13)$] and 2 rotation-electronic (**L**-uncoupling) parameters of the A$^1\Pi(v = 3)$ ~ [I$^1\Sigma^-(v = 5)$, D$^1\Delta(v = 4)$] interactions. The final model includs 5 unimolecular interactions, which had not been taken into account previously. The precision of the A$^1\Pi(v = 3)$ term values determined in this work is improved by a factor of 10 relative to the previously known values [40]. A significant, indirect influence of a$^3\Pi(v = 14)$ on A$^1\Pi(v = 3)$ via the e$^3\Sigma^-(v = 6)$ mediating level and a'$^3\Sigma^+(v = 14)$ on e$^3\Sigma^-(v = 6)$ via the A$^1\Pi(v = 3)$ level in ^{12}C^{18}O were detected. In addition, it has been shown that the A$^1\Pi(v = 3)$ ~ d$^3\Delta(v = 8)$ interaction, used in the fit in Ref. [40], is actually too weak to be significant, even within the current, much improved measurement accuracy.

Order of magnitude advances in the resolution, sensitivity, and access to higher-J rotational levels have revealed qualitatively new classes of features in the spectrum. Foremost among these is the occurrence of perturbations between pairs of electronic-vibrational levels that, for reason of electronic selection rules or small vibrational overlap, should have been unobservable. We report observation and fitting of several examples of these *nominally unobservable perturbations*. They represent an important new class of perturbation: *mediated perturbations.* For such phenomenon two states, 1 and 2, cannot undergo a direct currently detectable perturbation since the interaction matrix element $< 1|\mathbf{H}|2 >$ is too small. However, states 1 and 2 can be simultaneously detectably perturbed by state 3, via a mediated interaction $< 1|\mathbf{H}'|3><3|\mathbf{H}''|2>$, which is then of much larger size than 0.01 cm^{-1}.

Many of such tiny orphan effects in the spectrum are now observable and assignable. These orphans can have previously unimagined dynamical and collisional consequences. This is an important necessary step toward the goal of a global deperturbation analysis of all electronic states, all isotopologues, and extended ranges of vibrational and rotational levels of CO, as well as a users' guide for extension to other important molecules.

CRediT authorship contribution statement

M.I. Malicka: Writing – review & editing, Writing – original draft, Visualization, Validation, Software, Methodology, Investigation, Formal analysis, Data curation. **R.W. Field:** Writing – review & editing, Writing – original draft, Validation, Funding acquisition, Conceptualization. **S. Ryzner:** Writing – review & editing, Visualization, Validation, Software, Formal analysis, Data curation. **A. Stasik:** Writing – review & editing, Visualization. **W. Ubachs:** Writing – review & editing, Validation. **A.N. Heays:** Writing – review & editing, Visualization, Validation, Investigation, Funding acquisition, Formal analysis. **N. de Oliveira:** Writing – review & editing, Writing – original draft, Investigation. **W. Szajna:** Writing – review & editing, Validation. **R. Hakalla:** Writing – review & editing, Writing – original draft, Visualization, Validation, Supervision, Software, Resources, Project administration, Methodology, Funding acquisition, Formal analysis, Conceptualization.

Declaration of competing interest

The authors declare that they have no known competing financial interests or personal relationships that could have appeared to influence the work reported in this paper.

Data availability

Data will be made available on request.

Acknowledgments

RH thanks LASERLAB-EUROPE for support of this research [grant numbers EUH2020-RIP-654148 and EC's-SPF-284464]. RH, MIM, SR, WSz, and AS thank European Regional Development Fund and the Polish state budget within the framework of the Carpathian Regional Operational Programme [grant number RPPK.01.03.0 0-18-0 01/10] through the funding of the Centre for Innovation and Transfer of Natural Sciences and Engineering Knowledge of the University of Rzeszów. AH acknowledges grant funding from the CAAS ERDF/ESF "Centre of Advanced Applied Sciences" (number CZ.02.1.01/0.0/0.0/16_019/0 0 0 0778). R.W. Field thanks the US National Science Foundation (grant number CHE-1800410) for support of his research, which includes substantial collaborations. The authors are grateful to the general and technical staff of SOLEIL synchrotron for running the facility and providing beam time under project numbers 20120653 and 20160118.

Appendix A. Supplementary material

Supplementary data to this article can be found online at https://doi.org/10.1016/j.saa.2024.124011.

References

[1] M. Eidelsberg, F. Rostas, Spectroscopic, absorption and photodissociation data for CO and isotopic-species between 91 and 115 nm, Astron. Astrophys. 235 (1990) 472–489.

[2] S. Kong, C.J. Lada, E.A. Lada, C. Román-Zúñiga, J.H. Bieging, M. Lombardi, J. Forbrich, J.F. Alves, The relationship between the dust and gas-phase CO across the california molecular cloud, Astrophys. J. 805 (2015) 58, https://doi.org/10.1088/0004-637X/805/1/58.

[3] K.M. Flaherty, A.M. Hughes, K.A. Rosenfeld, S.M. Andrews, E. Chiang, J.B. Simon, S. Kerzner, D.J. Wilner, Weak turbulence in the HD 163296 protoplanetary disk revealed by alma CO observations, Astrophys. J. 813 (2015) 99, https://doi.org/10.1088/0004-637X/813/2/99.

[4] A.D. Bolatto, S.R. Warren, A.K. Leroy, F. Walter, S. Veilleux, E.C. Ostriker, J. Ott, M. Zwaan, D.B. Fisher, A. Weiss, E. Rosolowsky, J. Hodge, Suppression of star formation in the galaxy NGC 253 by a starburst-driven molecular wind, Nature 499 (2013) 450–453, https://doi.org/10.1038/nature12351.

[5] R.T. Garrod, S.L.W. Weaver, E. Herbst, Complex chemistry in star-forming regions: An expanded gas-grain warm-up chemical model, Astrophys. J. 682 (2008) 283–302, https://doi.org/10.1086/588035.

[6] J.R. Lyons, E.D. Young, CO self-shielding as the origin of oxygen isotope anomalies in the early solar nebula, Nature 435 (2005) 317–320, https://doi.org/10.1038/nature03557.

[7] E. Bayet, M. Gerin, T.G. Phillips, A. Contursi, A survey of submillimeter C and CO lines in nearby galaxies, Astron. Astrophys. 460 (2006) 467–485, https://doi.org/10.1051/0004-6361:20053872.

[8] A. Abergel, P.A.R. Ade et al., Planck 2013 results. XI. All-sky model of thermal dust emission, Astron. Astrophys. 571 (2014) A11. 10.1051/0004-6361/201323195.

[9] H.A. Weaver, P.D. Feldman, M.F. A'Hearn, N. Dello Russo, S.A. Stern, The carbon monoxide abundance in comet 103P/Hartley 2 during the epoxi flyby, Astrophys. J. Lett. 734 (2011) L5, https://doi.org/10.1088/2041-8205/734/1/L5.

[10] T.M. Dame, D. Hartmann, P. Thaddeus, The milky way in molecular clouds: A new complete CO survey, Astrophys. J. 547 (2001) 792–813, https://doi.org/10.1086/318388.

[11] R. Farrenq, G. Guelachvili, A.J. Sauval, N. Grevesse, C.B. Farmer, Improved Dunham coefficients for CO from infrared solar lines of high rotational-excitation, J. Mol. Spectrosc. 149 (1991) 375–390, https://doi.org/10.1016/0022-2852(91)90293-J.

[12] D.C. Catling, 10.13 - Planetary Atmospheres, in: G. Schubert (Ed.), Treatise Geophys. Second Ed., Elsevier, Oxford, 2015, pp. 429–472. 10.1016/B978-0-444-53802-4.00185-8.

[13] H. Gao, Molecular photodissociation in the vacuum ultraviolet region: implications for astrochemistry and planetary atmospheric chemistry, Mol. Phys. 119 (2021) e1861354.

[14] Q.M. Konopacky, T.S. Barman, B.A. Macintosh, C. Marois, Detection of carbon monoxide and water absorption lines in an exoplanet atmosphere, Science 339 (2013) 1398–1401, https://doi.org/10.1126/science.1232003.

[15] M. Daprà, M.L. Niu, E.J. Salumbides, M.T. Murphy, W. Ubachs, Constraint on a cosmological variation in the proton-to-electron mass ratio from electronic CO absorption, Astrophys. J. 826 (2016) 192, https://doi.org/10.3847/0004-637X/826/2/192.

[16] A.J. de Nijs, E.J. Salumbides, K.S.E. Eikema, W. Ubachs, H.L. Bethlem, UV-frequency metrology on CO a$^3\Pi$: Isotope effects and sensitivity to a variation of the proton-to-electron mass ratio, Phys. Rev. A 84 (2011) 052509, https://doi.org/10.1103/PhysRevA.84.052509.

[17] E.J. Salumbides, M.L. Niu, J. Bagdonaite, N. de Oliveira, D. Joyeux, L. Nahon, W. Ubachs, CO A-X system for constraining cosmological drift of the proton-electron mass ratio, Phys. Rev. A 86 (2012) 022510, https://doi.org/10.1103/PhysRevA.86.022510.

[18] P. Jansen, H.L. Bethlem, W. Ubachs, Perspective: Tipping the scales: Search for drifting constants from molecular spectra, J. Chem. Phys. 140 (2014) 010901, https://doi.org/10.1063/1.4853735.

[19] Y. Sheffer, S.R. Federman, D.L. Lambert, J.A. Cardelli, Fractionation of CO in the diffuse clouds toward zeta ophiuchi, Astrophys. J. 397 (1992) 482–491, https://doi.org/10.1086/171805.

[20] D.L. Lambert, Y. Sheffer, R.L. Gilliland, S.R. Federman, Interstellar carbon monoxide toward zeta-Ophiuchi, Astrophys. J. 420 (1994) 756–771, https://doi.org/10.1086/173600.

[21] C.H. Lyu, A.M. Smith, F.C. Bruhweiler, A statistical equilibrium analysis of interstellar CO toward zeta Ophiuchi as recorded by the goddard high resolution spectrograph, Astrophys. J. 426 (1994) 254–268, https://doi.org/10.1086/174060.

[22] J.L. Fox, Models for aurora and airglow emissions from other planetary-atmospheres, Can. J. Phys. 64 (1986) 1631–1656, https://doi.org/10.1139/p86-288.

[23] K. Bielska, A.A. Kyuberis, Z.D. Reed, G. Li, A. Cygan, R. Ciurylo, E.M. Adkins, L. Lodi, N.F. Zobov, V. Ebert, D. Lisak, J.T. Hodges, J. Tennyson, O.L. Polyansky, Subpromille measurements and calculations of CO (3–0) overtone line intensities, Phys. Rev. Lett. 129 (2022) 043002, https://doi.org/10.1103/PhysRevLett.129.043002.

[24] A. Cygan, S. Wójtewicz, G. Kowzan, M. Zaborowski, P. Wcislo, J. Nawrocki, P. Krehlik, L. Sliwczynski, M. Lipinski, P. Maslowski, R. Ciurylo, D. Lisak, Absolute molecular transition frequencies measured by three cavity-enhanced spectroscopy techniques, J. Chem. Phys. 144 (2016) 214202, https://doi.org/10.1063/1.4952651.

[25] I.E. Gordon, L.S. Rothman, C. Hill, R.V. Kochanov, Y. Tan, P.F. Bernath, M. Birk, et al., The HITRAN2016 molecular spectroscopic database, J. Quan.t Spectros. Radiat. Transf. 203 (2017) 3–69, https://doi.org/10.1016/j.jqsrt.2017.06.038.

[26] F. Rostas, M. Eidelsberg, A. Jolly, J.L. Lemaire, A. Le Floch, J. Rostas, Band oscillator strengths of the intersystem transitions of CO, J. Chem. Phys. 112 (2000) 4591–4603, https://doi.org/10.1063/1.481082.

[27] M. Eidelsberg, F. Rostas, An atlas of the intersystem transitions of CO, Astrophys. J. Suppl. Ser. 145 (2003) 89–109, https://doi.org/10.1086/345596.

[28] M. Eidelsberg, J.L. Lemaire, J.H. Fillion, F. Rostas, S.R. Federman, Y. Sheffer, Oscillator strengths for transitions to Rydberg levels in $^{12}C^{16}O$,$^{13}C^{16}O$ and $^{13}C^{18}O$ between 967 and 972 Å, Astron. Astrophys. 424 (2004) 355–361, https://doi.org/10.1051/0004-6361:20041017.

[29] M. Eidelsberg, F. Launay, K. Ito, T. Matsui, P.C. Hinnen, E. Reinhold, W. Ubachs, K. P. Huber, Rydberg-valence interactions of CO, and spectroscopic evidence characterizing the $C'^1\Sigma^+$ valence state, J. Chem. Phys. 121 (2004) 292–308, https://doi.org/10.1063/1.1756579.

[30] M. Eidelsberg, J.L. Lemaire, S.R. Federman, G. Stark, Heays A.N., Y. Sheffer, L. Gavilan, J.H. Fillion, F. Rostas, J.R. Lyons, P.L. Smith, N. de Oliveira, D. Joyeux, M. Roudjane, L. Nahon, High-resolution study of oscillator strengths and predissociation rates for $^{12}C^{16}O$, Astron. Astrophys. 543 (2012) A69. 10.1051/0004-6361/201118766.

[31] M. Eidelsberg, J.L. Lemaire, S.R. Federman, G. Stark, A.N. Heays, L. Gavilan, J. R. Lyons, P.L. Smith, N. de Oliveira, D. Joyeux, High-resolution study of oscillator strengths and predissociation rates for $^{13}C^{16}O$ and $^{12}C^{18}O$ W- X bands and Rydberg complexes in the 92.5-97.5 nm range, Astron. Astrophy. 566 (2014) A96, https://doi.org/10.1051/0004-6361/201423453.

[32] A.N. Heays, A.D. Bosman, E.F. van Dishoeck, Photodissociation and photoionisation of atoms and molecules of astrophysical interest, Astron. Astrophy. 602 (2017) A105, https://doi.org/10.1051/0004-6361/201628742.

[33] H. Lefebvre-Brion, R.W. Field, The spectra and dynamics of diatomic molecules, in: The Spectra and Dynamics of Diatomic Molecules, Elsevier, 2004, pp. 621– 739, 10.1016/B978-012441455-6/50012-3.

[34] R. Hakalla, M.L. Niu, R.W. Field, E.J. Salumbides, A.N. Heays, G. Stark, J.R. Lyons, et al., VIS and VUV spectroscopy of $^{12}C^{17}O$ and deperturbation analysis of the $A^1\Pi$, ν=1-5 levels, RSC Adv. 6 (2016) 31588–31606, https://doi.org/10.1039/C6RA01358A.

[35] R. Hakalla, M.L. Niu, R.W. Field, A.N. Heays, E.J. Salumbides, G. Stark, J.R. Lyons, et al., Fourier-transform spectroscopy of $^{13}C^{17}O$ and deperturbation analysis of the $A^1\Pi$ (v=0-3) levels, J. Quant. Spectrosc. Radiat. Transf. 189 (2017) 312–328, https://doi.org/10.1016/j.jqsrt.2016.12.012.

[36] R. Hakalla, T.M. Trivikram, A.N. Heays, E.J. Salumbides, N. de Oliveira, R. W. Field, W. Ubachs, Precision spectroscopy and comprehensive analysis of perturbations in the $A^1\Pi$ (v=0) state of $^{13}C^{18}O$, Mol. Phys. 117 (2019) 79–96, https://doi.org/10.1080/00268976.2018.1495848.

[37] M.I. Malicka, S. Ryzner, A.N. Heays, N. de Oliveira, R.W. Field, W. Ubachs, R. Hakalla, Deperturbation analysis of the $A^1\Pi$ (ν=2) level in the $^{12}C^{18}O$ isotopologue, J. Quant. Spectrosc. Radiat. Transf. 273 (2021) 107837, https://doi.org/10.1016/j.jqsrt.2021.107837.

[38] S. Ryzner, M.I. Malicka, A.N. Heays, R.W. Field, N. de Oliveira, W. Szajna, W. Ubachs, R. Hakalla, VUV-VIS FT spectroscopy of the rare of $^{13}C^{18}O$ isotopologue of carbon monoxide: Analysis of the $A^1\Pi$ (v=1) multiply-perturbed level, Spectrochim. Acta A Mol. Biomol. Spectrosc. 279 (2022) 121367, https://doi.org/10.1016/j.saa.2022.121367.

[39] C. Haridass, S.P. Reddy, A.C. Le Floch, The fourth positive ($A^1\Pi$ - $X^1\Sigma^+$) system of $^{12}C^{18}O$ and $^{13}C^{18}O$: Perturbations in the $A^1\Pi$ state, J. Mol. Spectrosc. 167 (1994) 334–352, https://doi.org/10.1006/jmsp.1994.1240.

[40] L.M. Beaty, V.D. Braun, K.P. Huber, A.C. Le Floch, A high-resolution ^{18}O isotope study in the vacuum ultraviolet of the $A^1\Pi$ - $X^1\Sigma^+$ 4th positive system of CO, Astrophys. J., Suppl. Ser. 109 (1997) 269–277, https://doi.org/10.1086/312976.

[41] T.M. Trivikram, R. Hakalla, A.N. Heays, M.L. Niu, S. Scheidegger, E.J. Salumbides, N. de Oliveira, R.W. Field, W. Ubachs, Perturbations in the $A^1\Pi$, v=0 state of $^{12}C^{18}O$ investigated via complementary spectroscopic techniques, Mol. Phys. 115 (2017) 3178–3191, https://doi.org/10.1080/00268976.2017.1356477.

[42] M.I. Malicka, S. Ryzner, A.N. Heays, N. de Oliveira, R.W. Field, W. Ubachs, R. Hakalla, High-resolution Fourier-transform spectroscopy and deperturbation analysis of the $A^1\Pi$ (ν=1) level in $^{12}C^{18}O$, J. Quant. Spectrosc. Radiat Transf. 255 (2020) 107243, https://doi.org/10.1016/j.jqsrt.2020.107243.

[43] M.L. Niu, E.J. Salumbides, D. Zhao, N. de Oliveira, D. Joyeux, L. Nahon, R.W. Field, W. Ubachs, High resolution spectroscopy and perturbation analysis of the CO $A^1\Pi$ - $X^1\Sigma^+$ (0,0) and (1,0) bands, Mol. Phys. 111 (2013) 2163–2174, https://doi.org/10.1080/00268976.2013.793889.

[44] M.L. Niu, E.J. Salumbides, A.N. Heays, N. de Oliveira, R.W. Field, W. Ubachs, Spectroscopy and perturbation analysis of the CO $A^1\Pi$ - $X^1\Sigma^+$ (2,0), (3,0) and (4,0) bands, Mol. Phys. 114 (2016) 627–636, https://doi.org/10.1080/00268976.2015.1108472.

[45] N. de Oliveira, M. Roudjane, D. Joyeux, D. Phalippou, J.C. Rodier, L. Nahon, High-resolution broad-bandwidth Fourier-transform absorption spectroscopy in the VUV range down to 40 nm, Nat. Photonics 5 (2011) 149–153, https://doi.org/10.1038/NPHOTON.2010.314.

[46] N. de Oliveira, D. Joyeux, M. Roudjane, J.F. Gil, B. Pilette, L. Archer, K. Ito, L. Nahon, The high-resolution absorption spectroscopy branch on the VUV beamline DESIRS at SOLEIL, J. Synchrotron Radiat. 23 (2016) 887–900, https://doi.org/10.1107/S1600577516006135.

[47] M.L. Niu, A.N. Heays, S. Jones, E.J. Salumbides, E.F. van Dishoeck, N. de Oliveira, L. Nahon, W. Ubachs, VUV-synchrotron absorption studies of N_2 and CO at 900 K, J. Mol. Spectrosc. 315 (2015) 137–146, https://doi.org/10.1016/j.jms.2015.02.011.

[48] F. Li, R. Klette, Analysis of the rubberband algorithm, Image Vis. Comput. 25 (2007) 1588–1598, https://doi.org/10.1016/j.imavis.2006.06.021.

[49] Bruker, OPUS: spectroscopy software for state-of-the-art measurement, processing and evaluation of IR, NIR and Raman Spectra. v.8.5.29., Bruker Optik GmbH, 2019.

[50] R. Hakalla, M. Zachwieja, W. Szajna, First analysis of the 1–v″ progression of the Ångström ($B^1\Sigma^+$ - $A^1\Pi$) band system in the rare $^{13}C^{17}O$ isotopologue, J. Phys. Chem. A 117 (2013) 12299–12312, https://doi.org/10.1021/jp4077239.

[51] R. Hakalla, W. Szajna, M. Zachwieja, R. Kepa, Reanalysis of the Ångström System ($B^1\Sigma^+$ - $A^1\Pi$) in the $^{13}C^{16}O$ Isotopic Molecule, Acta Phys. Pol. A. 122 (2012) 674–682. 10.12693/APhysPolA.122.674.

[52] R.A. Toth, Line-frequency measurements and analysis of N_2O between 900 and 4700 cm $^{-1}$, Appl. Opt. 30 (1991) 5289–5315, https://doi.org/10.1364/AO.30.005289.

[53] A. Keens, IFS120HR manual, III. Acceptance Specifications, C. Mid IR Region, Bruker Optik GmbH, 2010.

[54] R. Kepa, M. Ostrowska-Kopec, I. Piotrowska, M. Zachwieja, R. Hakalla, W. Szajna, P. Kolek, Ångström ($B^1\Sigma^+ \rightarrow A^1\Pi$) 0–1 and 1–1 bands in isotopic CO molecules: further investigations, J. Phys. B-At. Mol. Opt. 47 (2014) 045101, https://doi.org/10.1088/0953-4075/47/4/045101.

[55] M. Eidelsberg, J.Y. Roncin, A. Le Floch, F. Launay, C. Letzelter, J. Rostas, Reinvestigation of the vacuum ultraviolet-spectrum of CO and isotopic-species – the $B^1\Sigma^+ \leftrightarrow X^1\Sigma^+$ transition, J. Mol. Spectrosc. 121 (1987) 309–336, https://doi.org/10.1016/0022-2852(87)90055-5.

[56] W. Ubachs, P.C. Hinnen, P. Hansen, S. Stolte, W. Hogervorst, P. Cacciani, Laser spectroscopic studies of the $C^1\Sigma^+$, (v = 0) and (v = 1) states of CO, J. Mol. Spectrosc. 174 (1995) 388–396, https://doi.org/10.1006/jmsp.1995.0010.

[57] R.W. Field, Spectroscopy and Perturbation Analysis in Excited States of CO and CS, PhD Thesis, Harvard University, 1971.

[58] J.A. Coxon, P.G. Hajigeorgiou, Direct potential fit analysis of the $X^1\Sigma^+$ ground state of CO, J. Chem. Phys. 121 (2004) 2992–3008, https://doi.org/10.1063/1.1768167.

[59] A.C. Le Floch, F. Launay, J. Rostas, R.W. Field, C.M. Brown, K. Yoshino, Reinvestigation of the CO $A^1\Pi$ state and its perturbations – the v=0 levels, J. Mol. Spectrosc. 121 (1987) 337–379, https://doi.org/10.1016/0022-2852(87)90056-7.

[60] S.G. Tilford, R.A. Howard, M.L. Ginter, Fluorescence of carbon-monoxide excited by 1306-Å oxygen resonance line, J. Chem. Phys. 56 (1972) 1413–1415, https://doi.org/10.1063/1.1677380.

[61] C. Kittrell, B.A. Garetz, Analysis of the $D^1\Delta$ - $X^1\Sigma^+$ transition in CO observed by two-photon excitation, Spectrochim. Acta A Mol. Biomol. Spectrosc. 45 (1989) 31–40, https://doi.org/10.1016/0584-8539(89)80024-8.

[62] G.L. Wolk, J.W. Rich, Observation of a new electronic state of carbon-monoxide using LIF on highly vibrationally excited CO ($X^1\Sigma^+$), J. Chem. Phys. 79 (1983) 12–18, https://doi.org/10.1063/1.445571.

[63] G.J. Vázquez, J.M. Amero, H.P. Liebermann, H. Lefebvre-Brion, Potential energy curves for the $^1\Sigma^+$ and $^{1,3}\Pi$ states of CO, J. Phys. Chem. A. 113 (2009) 13395–13401, https://doi.org/10.1021/jp902730d.

[64] R. Kępa, New spectroscopic studies of the Herzberg bands of the $^{12}C^{16}O$ molecule, J. Mol. Spectrosc. 135 (1989) 119–130, https://doi.org/10.1016/0022-2852(89)90359-7.

[65] K.P. Huber, G. Herzberg, Constants of diatomic molecules, in: K.P. Huber, G. Herzberg (Eds.), Molecular Spectra and Molecular Structure: IV. Constants of Diatomic Molecules, Springer US, Boston, MA, 1979: pp. 8–689. 10.1007/978-1-4757-0961-2_2.

[66] T. Rytel, Analysis of the perturbed 2–2 band of the third positive ($b^3\Sigma^+$- $a^3\Pi_r$) system of CO, J. Mol. Spectrosc. 151 (1992) 271–274, https://doi.org/10.1016/0022-2852(92)90563-4.

[67] C. Western, PGOPHER: A program for simulating rotational, vibrational and electronic spectra, J. Quant. Spectrosc. Radiat. Transf. 186 (2017) 221–242, https://doi.org/10.1016/j.jqsrt.2016.04.010.

[68] C.M. Western PGOPHER: Simulates Rotational, Vibrational and Electronic Spectra.11.0.142 (developed, beta version), Bristol: UK: University of Bristol; 2021. http://pgopher.chm.bris.ac.uk/pgopher-beta/.

[69] N. Åslund, A numerical-method for simultaneous determination of term values and molecular-constants, J. Mol. Spectrosc. 50 (1974) 424–434, https://doi.org/10.1016/0022-2852(74)90245-8.

[70] R.F. Curl, C.B. Dane, Unbiased least-squares fitting of lower states, J. Mol. Spectrosc. 128 (1988) 406–412, https://doi.org/10.1016/0022-2852(88)90157-9.

[71] J.K.G. Watson, On the use of term values in the least-squares fitting of spectra, J. Mol. Spectrosc. 138 (1989) 302–308, https://doi.org/10.1016/0022-2852(89)90119-7.

[72] C. Focsa, A. Poclet, B. Pinchemel, R.J. Le Roy, P.F. Bernath, Fourier transform spectroscopy of the $A'^1\Pi$ - $X^1\Sigma^+$ system of CaO, J. Mol. Spectrosc. 203 (2000) 330–338, https://doi.org/10.1006/jmsp.2000.8187.

[73] R.W. Field, J.D. Simmons, S.G. Tilford, B.G. Wicke, Analysis of perturbations in the $a^3\Pi$ and $A^1\Pi$ states of CO, J. Mol. Spectrosc. 44 (1972) 383–399, https://doi.org/10.1016/0022-2852(72)90111-7.

[74] S. Yamamoto, S. Saito, The microwave spectra of CO in the electronically excited states $a^3\Pi$ and $a'^3\Sigma^+$, J. Chem. Phys. 89 (1988) 1936–1944, https://doi.org/10.1063/1.455091.

[75] B.A. Garetz, C. Kittrell, A.C. Le Floch, Analysis of the two-photon $D^1\Delta$ – $X^1\Sigma^+$ transition in CO: Perturbations in the (10–0) band, J. Chem. Phys. 94 (1991) 843–853, https://doi.org/10.1063/1.459973.

[76] J.D. Simmons, S.G. Tilford, Observation of $D^1\Delta$-$X^1\Sigma^+$ transition of CO in vacuum-ultraviolet region, J. Chem. Phys. 45 (1966) 2965–2968, https://doi.org/10.1063/1.1728052.

[77] P.H. Krupenie, The Band Spectrum of Carbon Monoxide. National Standard Reference Data Series, NBS-5 1966.

[78] M. Rytel, Ångström system of the $^{12}C^{18}O$ molecule, Acta Phys. Pol. 38 (1970) 299–308.

[79] J.D. Janjić, L.J.U. Conkic, D.S. Pesic, R. Kępa, M. Rytel, Herzberg system of $^{12}C^{18}O$ molecule, J. Mol. Spectrosc. 72 (1978) 297–300, https://doi.org/10.1016/0022-2852(78)90130-3.

[80] A. Du Plessis, E.G. Rohwer, C.M. Steenkamp, Accurate laboratory wavelengths of the $A^1\Pi$(v'=0-5) - $X^1\Sigma^+$(v''=0) vibronic bands of $^{12}C^{17}O$ and $^{12}C^{18}O$, Astrophys. J., Suppl. Ser. 165 (2006) 432–437, https://doi.org/10.1086/504428.

[81] A. Du Plessis, E.G. Rohwer, C.M. Steenkamp, Investigation of four carbon monoxide isotopomers in natural abundance by laser-induced fluorescence in a supersonic jet, J. Mol. Spectrosc. 243 (2007) 124–133, https://doi.org/10.1016/j.jms.2007.01.009.

[82] C.M. Steinmann, E.G. Rohwer, H. Stafast, Accurate laboratory wavelengths of the vacuum ultraviolet A(v' = 3) - X(v'' = 0) band $^{12}C^{17}O$ and $^{12}C^{18}O$, Astrophys. J. 590 (2003) L123–L126, https://doi.org/10.1086/376750.

[83] R.W. Field, S.G. Tilford, J.D. Simmons, R.A. Howard, Fine structure and perturbation analysis of $a^3\Pi$ state of CO, J. Mol. Spectrosc. 44 (1972) 347–382, https://doi.org/10.1016/0022-2852(72)90110-5.